Contrib Mineral Petrol (2006) 152: 53–74
DOI 10.1007/s00410-006-0094-3

ORIGINAL PAPER

Xie-Yan Song · Mei-Fu Zhou · Reid R. Keays
Zhi-Min Cao · Min Sun · Liang Qi

Geochemistry of the Emeishan flood basalts at Yangliuping, Sichuan, SW China: implications for sulfide segregation

Received: 5 December 2005 / Accepted: 21 March 2006 / Published online: 3 June 2006

Abstract A well-developed, 1,000 m thick basaltic sequence in the Yangliuping region, northern part of the Emeishan basalt province, includes the Lower and Middle Units of tholeiitic basalts and an Upper Unit of both tholeiites and subalkalic basalts. The basalts contain 42–55 wt% SiO_2 and 4.1–8.3 wt% MgO. Most of these lavas have Gd/Yb > 2.0, Zr/Nb < 12, and $\varepsilon_{Nd(260\ Ma)}$ values from +2.5 to +4.7. The platinum-group elements (PGE) are very mildly depleted in most of the basalts which contain 8–19 ppb Pt and 7–27 ppb Pd. However, a significant proportion of the Middle Unit basalts are strongly depleted in PGE with some samples having concentrations lower than detection limits. They have extremely high Zr/Nb ratios (up to 14.5) and low $\varepsilon_{Nd(260\ Ma)}$ values (+3.21 to +0.65), features of extensive lower crustal contamination. Some samples in this unit have high Ni/Pd (3,965–61,198) and low Pd/Cr (410,000–3,930,000) ratios, indicating sulfide segregation and PGE depletion prior to eruption. The primary magmas were S-undersaturated and derived from partial melting at variable depths in the upper mantle. The early and late stage magmas, as represented by the Lower and Upper Units, underwent AFC processes which induced mild S-saturation and PGE depletion in some of the basalts, whereas the magmas represented by the Middle Unit experienced more extensive crustal contamination resulting in stronger S-saturation and in most cases significant PGE depletion.

Communicated by J. Hoefs

X.-Y. Song (✉)
State Key Laboratory of Ore Deposit Geochemistry,
Institute of Geochemistry, Chinese Academy of Sciences,
64th Guanshui Road, Guiyang 550002,
People's Republic of China
E-mail: songxieyan@vip.gyig.ac.cn
Tel.: +86-851-5895538
Fax: +86-851-5895538

M.-F. Zhou · M. Sun · L. Qi · X.-Y. Song
Department of Earth Sciences, The University of Hong Kong,
Hong Kong, People's Republic of China

R. R. Keays
School of Geosciences, Monash University,
PO Box 28E, Monash, VIC 3800, Australia

R. R. Keays
Mineral Exploration Research Center, Laurentian University,
Sudbury, ON, Canada P3E 2C6

Z.-M. Cao
College of Earth Sciences, Ocean University of China,
Qingdao 266003, People's Republic of China

Introduction

The Emeishan Large Igneous Province (ELIP) cover large areas in SW China and Northern Vietnam and include the Emeishan continental flood basalts (ECFB) (Song et al. 2001) and mafic–ultramafic intrusions that have been dated at 260 Ma (Zhou et al. 2002a, 2006; Guo et al. 2004). Numerous magmatic Ni–Cu–(PGE) (platinum-group elements) sulfide deposits, such as the Yangliuping, Limahe, and Jinbaoshan deposits, are hosted in conformable mafic–ultramafic sills or disconformable bodies (e.g., Zhou et al. 2002b; Song et al. 2003, 2004a) (Fig. 1). Some layered intrusions in the ELIP host V–Ti magnetite deposits, such as the Hongge and Panzhihua intrusions (Fig. 1) (Zhong et al. 2002; Zhou et al. 2005). The magnetite deposits and most of the magmatic sulfide deposits are distributed in the central part of the ELIP (Song et al. 2005a, b). However, the temporal evolution of the basaltic magmas and a potential genetic link with the formation of Ni–Cu–(PGE) sulfide deposits has not been well addressed.

In the Yangliuping area, some differentiated mafic–ultramafic sills contain Ni–Cu–(PGE) sulfide ores and are spatially associated with the Permian ECFB (Zhou et al. 2002b; Song et al. 2003) (Fig. 2). Petrographic and geochemical data of rocks from the differentiated sills in

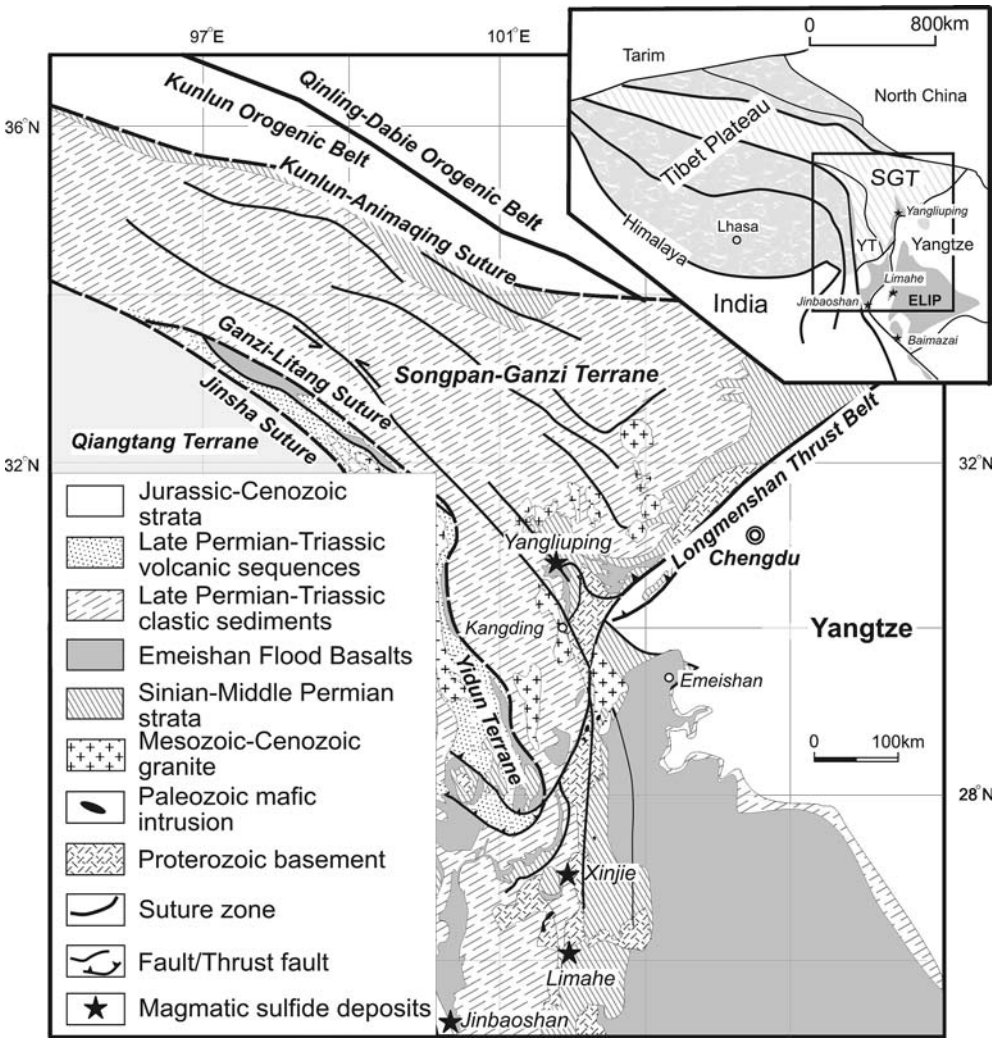

Fig. 1 Regional geological map of the Songpan-Ganzi Terrane and northern part of the Emeishan Large Igneous Province showing the location of the Yangliuping area. Modified from the regional geological maps of Sichuan, Yunnan, and Qinghai Provinces, SW China (adopted from X.-Y. Song, unpublished data). *SGT* Songpan-Ganzi Terrane, *YT* Yidun Terrane

the Yangliuping area indicate that the sulfide mineralization resulted from segregation of immiscible sulfide melts in the magma conduits that later solidified as sills (Song et al. 2003; X.-Y. Song, unpublished data). The spatial and temporal associations between the Permian lavas and the mafic–ultramafic intrusions provide a good opportunity to study the genetic links between the magmatic evolution of the lavas and concentrations of Ni, Cu, and PGE in the co-magmatic subvolcanic intrusions.

In this paper, we report major and trace elements, PGE, and Nd isotope compositions for volcanic lavas from a cross-section in the Yangliuping region. The data allow us to establish a comprehensive understanding of the petrogenesis of the Yangliuping basalts and to constrain the fractional crystallization, crustal contamination, and S-saturation history of the magmas. Our approach follows that developed by Naldrett et al. (1992, 1995), Hawkesworth et al. (1995), Lightfoot and Hawkesworth (1997), and Lightfoot and Keays (2005), who used geochemistry to decipher the relationships between mineralization, magmatic intrusions, and basaltic volcanism at Noril'sk in Russia.

Geological background

In the northeastern part of the Tibetan Plateau, the Songpan-Ganzi Terrane is separated from the Yangtze Block by the Longmenshan Thrust Belt in the east, from the Yidun Terrane by the Ganzi-Litang suture zone in the west, and from the North China Craton by the Kunlun and Qinling-Dabie Orogenic Belts in the north (Fig. 1) (Song et al. 2004a). The Neoproterozoic and Paleozoic rock assemblages along the eastern and southwestern margins of the Songpan-Ganzi Terrane are similar to those of the western Yangtze Block.

The ECFB extends from the western Yangtze Block to the eastern and southwestern margins of the Songpan-Ganzi Terrane and is mainly exposed along thrust faults and around tectonic domes (Fig. 1) (Chung and Jahn 1995; Song et al. 2001, 2004a; Xu et al. 2001; Zhou et al. 2002a; Ali et al. 2002). The Yangliuping region is located at the southwestern end of the Longmenshan Thrust Belt (Fig. 1). The Proterozoic and Paleozoic rocks are exposed in tectonic domes that occur along the axis of the NW–SE trending Danba anticline.

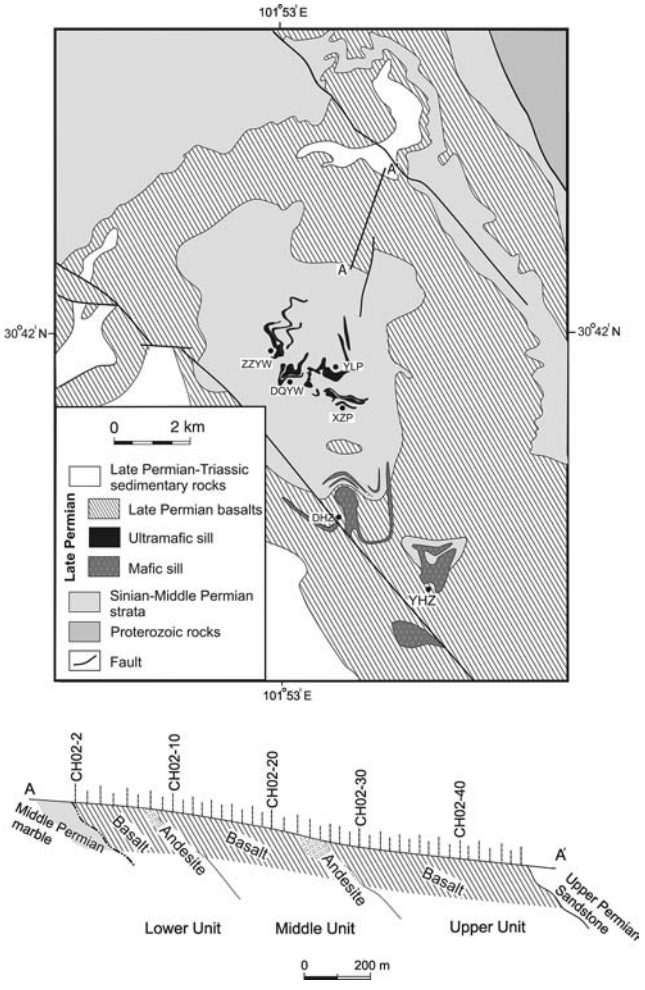

Fig. 2 Geological map of the Yangliuping dome (modified after BGMS 1982). The Ni–Cu–(PGE) (platinum-group elements) sulfide-bearing mafic–ultramafic sills intrude Devonian strata in the core of the dome, which is surrounded by the Late Permian flood basalts. The Yuhaizi dome is a small dome occurring in the southern limb of the Yangliuping dome that cuts Devonian–Early Permian strata and the Late Permian flood basalts. The mafic–ultramafic intrusions include: *YLP* Yangliuping sill, *ZZYW* Zhengziyanwuo sill, *XZP* Xiezuuoping sill, *DQYW* Daqiangyanwuo sill, *DHZ* Dahaizi sill, *YHZ* Yuhaizi intrusion. Cross-section of the Yangliuping basalts shows the subdivision of the Late Permian meta-lavas, which disconformably overlie the Middle Permian marble and are conformably overlain by the Late Permian meta-sandstone. The meta-basalts are subdivided into Lower, Middle, and Upper Units. The Lower and Middle Units consist of epidote–actinolite schist (meta-basalts) grading upward to epidote–albite–actinolite schist (meta-andesites). Geochemical samples are shown as CH02-*xx*

Sinian-Middle Permian rocks unconformably overlie the Proterozoic crystalline rocks and are disconformably overlain by the Late Permian ECFB. In the Yangliuping region, the ECFB is 1,000–2,500 m thick and extends southward to Kangding (Fig. 1). The basalts disconformably overlie Middle Permian marble and are overlain by Late Permian meta-sandstone, which are in turn conformably overlain by Triassic sedimentary rocks (Fig. 2).

There are more than 170 thin mafic sills (less than 30 m thick) and several well differentiated mafic–ultramafic sills (up to 300 m thick) in the Yangliuping area. Most of them intrude the Devonian to Permian strata along bedding planes but a few intrude strata as young as the lower part of the Permian basalts. The Yangliuping and Zhengziyanwuo sills host economic Ni–Cu–(PGE) sulfide deposits (Fig. 2). These two sills consist of serpentinite, talc schist, tremolite schist, and minor altered gabbro from the base to the top. Relict poikilitic textures are common in the serpentinite and talc schist, as manifested by the pseudomorphs of granular olivine within large grains of tremolite that replaced pyroxene. In the serpentinite, intergranular space may be filled with sulfides (Song et al. 2003, 2004b; X.-Y. Song, unpublished data) to form stratiform disseminated sulfide ore bodies ranging up to more than 1,000 m long and 20–50 m thick (locally up to 100 m). Sulfide concentrations in the disseminated ore bodies decrease from $>30\%$ at their bases to 10% upward. Massive sulfides occur in the base of the Yangliuping sill and locally extend to the footwall rock near the contact. The largest massive ore body is lenticular, about 200 m long and generally 2–5 m thick, and parallel to the base of the sill.

The Yangliuping basalt sequence has undergone greenschist facies metamorphism to form actinolite schist. It is divided into Lower, Middle and Upper Units (Fig. 2), and epidote–albite–actinolite schists dominate the tops of the Lower and Middle Units. Individual lava flows cannot be identified clearly. Porphyrititc, intersertal, and amygdaloidal textures are well preserved in the lavas at the southern part of the Yangliuping dome (Fig. 2). Relict intersertal textures, in which randomly oriented saussuritized plagioclase laths form a network and the interstitial material is replaced by epidote and chlorite, are observed in aphyric basalts and the matrix of porphyritic basalts. Porphyritic textures are common in the basalts with plagioclase phenocrysts. Amygdaloidal basalt occurs in the Lower Unit and the typical amygdules have a rim of chlorite, surrounding a core of quartz and calcite.

The Lower Unit consists of fine-grained, dark green and well-foliated epidote–actinolite schists (100 m thick) overlain by epidote–albite–actinolite schists (30 m thick). The epidote–actinolite schists consist of actinolite, biotite, albite, and epidote together with accessory sphene and magnetite. The epidote–albite–actinolite schists contain significantly more albite and less actinolite. These schists also contain biotite and epidote, with minor amounts of magnetite and sphene.

The Middle Unit consists of epidote–actinolite schists (300 m thick) overlain by epidote–albite–actinolite schists (60 m thick). Mineral assemblages of the schists are the same as those of the Lower Unit but larger variations in modal percentages. Relict magmatic plagioclase phenocrysts with polysynthetic twinning are preserved in many samples.

The Upper Unit (500 m thick) consists of dark green and fine-grained biotite–actinolite schist. Compared

with the epidote–actinolite schists of the Lower and Middle Units, the biotite–actinolite schists of the Upper Unit contain more actinolite and biotite and less epidote.

Sample preparation and analytical techniques

Forty-three samples were collected at intervals of 20–25 m from the bottom to the top of the Yangliuping basalt sequence. Weathered surface of the samples was removed.

Major oxide contents were determined by X-ray fluorescence spectrometry (XRF) on fused glass pellets. Trace elements, Sc, V, Cr, Ni, and Cu, were determined by XRF analysis on pressed powder pellets. Other trace elements, including rare earth elements (REE) were determined by inductively coupled plasma mass spectrometry (ICP-MS) at The University of Hong Kong. The ICP-MS analyses followed the technique of Jenner et al. (1990) using standard additions, pure elemental standards for external calibration, and BHVO-1 as a reference material. Accuracy and precision of the XRF analyses are estimated to be ±2% for major oxides present in concentrations greater than 0.5 wt% and ±5% for trace elements. Accuracy and precision of the ICP-MS analyses are better than ±5%. Contents of major oxides and trace elements in the Yangliuping basalts are given in Table 1.

The PGE analyses were carried out at the low-level PGE facility of the Geoscience Laboratories in Sudbury, following procedures described in Jackson et al. (1990). Fifteen grams of powdered sample were mixed with sodium carbonate, sulfur, SiO_2 flour, and Ni powder. This mixture was baked at 1,500°C for 1.5 h in a clay crucible. The Ni-sulfide button was dissolved and the PGE were collected by Te precipitation, and then re-dissolved in acid and their final concentrations determined by ICP-MS. The limits of detection (average blank + three standard deviations) for Ir, Ru, Rh, Pt, Pd, and Au are estimated to be 0.05, 0.3, 0.1, 0.4, 1.4, and 1.2 ppb, respectively. The concentrations of the majority of the samples from the Lower and Upper Units are above the detection limits for all elements except Ir, Ru, and Au for which some samples have concentrations close to the detection limit. In contrast, many samples from the Middle Unit have PGE contents lower than the detection limits. Replicate analyses of the reference standard WPR-1 yielded average values of 21.4 ppb Ru, 12.8 ppb Rh, 233 ppb Pd, 15.3 ppb Ir, 265 ppb Pt, and 38 ppb Au, with relative standard deviations up to 7% except for Rh and Au for which the relative standard deviations are 10 and 13%, respectively. The average element concentrations of replicate analyses of WPR-1 are within 10% of the certified value except Ir which is 13% lower.

For the Sm–Nd isotope analyses, sample powders were spiked with mixed isotope tracers (^{149}Sm and ^{146}Nd), dissolved in Teflon capsules with mixed acid of HF and HNO_3, and separated by conventional cation-exchange techniques. A VG-354 mass-spectrometer was used for the isotopic measurement at the Institute of Geology and Geophysics, Chinese Academy of Sciences, Beijing. The fractionation correction for Nd isotopic ratios was based on $^{146}Nd/^{144}Nd = 0.7219$. The Sm–Nd isotope data are listed in Table 2.

Analytical results

Effect of metamorphism and alteration

It is important to identify trace elements that remain immobile during metamorphism in order to use these elements to investigate the petrogenesis of the basalts (Arndt et al. 1989; Lesher and Arndt 1995; Lesher et al. 2001).

Both REE and high field strength elements (HFSEs), e.g., Nb, Ta, Y, and Ti, have high valences and electronegativities, small radii, and strong chemical bonds. Therefore, even if primary minerals hosting these elements are destroyed during metamorphism or hydrothermal alteration, these elements tend to be trapped in the structure of secondary minerals, and remain immobile. Thus, the ratios between these elements remain constant. Good linear correlations between La and other REE and HFSEs, such as Gd and Zr, indicate that the REE and HFSEs are immobile during the greenschist metamorphism and hydrothermal alteration that affected the Yangliuping lavas (Fig. 3a, b).

The PGE are generally immobile during hydrothermal alteration because of their high electronegativities (2.2), valences (2^+–4^+), and first ionization potential (5.4–9.1 eV) (Pauling 1960; Weast et al. 1986). The good correlations between Pd and Pt and La/Sm ratios of the lavas of the Lower and Upper Units indicate that the PGE were immobile during metamorphism and hydrothermal alteration in the Yangliuping basalts (Fig. 3c, d). The decreases of PGE in the Middle Unit resulted from sulfide segregation as discussed below. Thus, REE, HFSEs, and PGE can be used to investigate the petrogenesis of the Yangliuping basalts.

Chemostratigraphic variation of the lava sequence

The Lower and Middle Units consist dominantly of a series of porphyritic to intersertal tholeiitic basalts overlain by basaltic andesite or andesite at the tops, whereas the Upper Unit comprises tholeiitic and subalkaline basalts. Chemostratigraphic variations of the Yangliuping lava sequence are summarized in Fig. 4. In this diagram, SiO_2, TiO_2, MgO, and Ni contents reflect the degree of fractional crystallization, Gd/Yb and Ti/Y ratios help to identify differences of parental magmas, and Zr/Nb and $\varepsilon_{Nd(260\ Ma)}$ are used to monitor crustal contamination.

Table 1 Chemical compositions of the Yangliuping basalts

	Lower Unit							Middle Unit							
	CH02-2	CH02-3	CH02-4	CH02-5	CH02-6	CH02-7	CH02-8	CH02-9	CH02-10	CH02-11	CH02-12	CH02-13	CH02-14	CH02-15	CH02-16
Oxides (wt%)															
SiO_2	49.01	49.9	48.9	49.2	49.5	55.5	61.4	52.8	47.8	48.0	48.3	50.4	49.67	50.3	50.5
TiO_2	1.49	1.86	2.04	1.85	1.89	2.01	1.62	2.37	2.82	2.53	1.88	2.52	2.42	1.18	2.11
Al_2O_3	14.6	14.1	14.7	15.82	14.3	13.3	13.0	13.4	14.2	13.36	14.2	13.9	14.0	16.4	13.2
Fe_2O_3	13.1	13.4	13.5	10.4	13.3	10.2	8.2	12.4	14.7	13.9	13.3	13.3	13.7	12.1	13.0
MnO	0.17	0.19	0.21	0.20	0.20	0.14	0.11	0.17	0.21	0.21	0.19	0.20	0.21	0.16	0.17
MgO	6.94	6.20	6.31	4.09	6.20	6.33	2.76	4.86	5.90	5.65	6.89	6.48	6.94	4.24	8.26
CaO	8.81	11.33	11.69	14.62	10.78	8.47	8.00	9.33	6.44	10.16	11.60	8.45	8.45	11.99	8.40
Na_2O	2.44	1.68	2.23	1.48	2.65	2.39	2.43	2.76	4.22	3.49	2.30	3.13	2.86	2.33	2.84
K_2O	0.80	0.32	0.32	0.24	0.35	0.99	0.75	0.61	2.07	1.01	0.32	0.25	0.84	0.23	0.99
P_2O_5	0.13	0.19	0.20	0.17	0.19	0.23	0.23	0.30	0.45	0.37	0.18	0.30	0.28	0.21	0.25
LOI	1.61	0.47	0.58	1.68	0.51	0.72	0.42	0.46	0.46	0.99	0.41	1.10	0.53	0.49	0.34
Total	99.16	99.63	100.63	99.80	99.86	100.27	98.97	99.44	99.23	99.67	99.63	99.90	99.90	99.55	100.03
Trace elements (ppm)															
Sc	26.0	28.9	30.8	28.3	29.9	25.4	20.0	26.5	31.5	30.6	30.9	25.0	25.3	15.2	29.3
V	310	335	364	294	347	274	239	356	379	395	348	391	372	370	312
Cr	191	113	98	133	102	84	26	18	51	37	154	15	18	−2	72
Co	54.3	54.5	46.2	35.2	55.9	41.9	26.6	43.9	51.5	45.2	52.5	49.4	46.2	26.8	61.7
Ni	114	74	48	57	80	68	22	33	53	47	82	40	51	20	92
Cu	250	70	99	37	145	6	87	106	120	50	76	101	45	327	145
La	11.9	13.8	14.4	12.6	13.4	20.1	32.1	22.6	30.9	27.0	13.1	23.1	21.2	14.5	21.3
Ce	27.5	32.3	33.9	30.1	31.7	47.3	69.5	52.3	67.8	62.1	29.4	50.5	45.7	28.1	45.8
Pr	3.4	4.4	4.6	4.0	4.3	6.2	8.6	6.9	8.8	8.1	4.2	7.1	6.5	3.8	6.3
Nd	15.1	20.2	21.3	18.5	19.8	27.5	35.9	30.2	37.6	35.6	19.5	30.6	28.4	16.0	27.4
Sm	3.6	4.9	5.2	4.5	4.9	6.0	7.4	6.5	7.8	7.4	4.7	6.7	6.3	3.5	6.0
Eu	1.6	1.7	1.8	1.6	1.7	1.6	2.0	2.2	2.7	2.4	1.6	2.2	2.1	2.0	1.9
Gd	3.5	4.7	5.1	4.4	4.7	5.4	6.6	5.8	7.0	6.6	4.7	6.0	5.4	3.2	5.3
Tb	0.6	0.9	0.9	0.8	0.8	0.9	1.1	1.0	1.1	1.1	0.8	1.0	0.9	0.5	0.8
Dy	3.6	4.9	5.1	4.3	4.9	5.1	6.3	5.2	6.3	5.7	4.7	5.3	5.0	3.2	4.8
Ho	0.7	0.9	1.0	0.9	1.0	1.0	1.3	1.0	1.2	1.1	0.9	1.0	1.0	0.7	0.9
Er	1.9	2.5	2.7	2.3	2.5	2.7	3.6	2.7	3.2	3.0	2.5	2.7	2.5	1.8	2.5
Tm	0.2	0.3	0.3	0.3	0.3	0.3	0.5	0.3	0.4	0.4	0.3	0.3	0.3	0.2	0.3
Yb	1.6	2.1	2.2	1.9	2.1	2.2	3.3	2.2	2.6	2.5	2.1	2.3	2.1	1.5	2.0
Lu	0.2	0.3	0.3	0.3	0.3	0.3	0.5	0.3	0.4	0.4	0.3	0.3	0.3	0.2	0.3
Rb	25.4	1.0	0.9	1.7	1.2	27.5	19.4	11.7	45.6	19.4	1.9	1.5	19.0	0.7	23.2
Sr	351.3	500.7	267.4	455.1	393.9	539.0	571.3	634.5	334.1	383.8	457.7	206.3	398.2	481.0	314.0
Ba	319.4	66.8	44.7	58.5	62.8	450.1	361.1	205.4	964.8	455.0	82.2	57.7	376.1	44.9	296.2
Y	17.0	24.3	25.6	21.7	24.4	26.0	34.0	26.0	29.9	28.7	23.3	26.8	24.4	18.1	23.3
Nb	9.1	11.9	12.8	11.7	12.0	13.3	15.0	14.8	24.6	23.7	11.5	15.2	13.3	8.8	13.1
Ta	0.6	0.7	0.8	0.7	0.7	0.8	1.0	0.9	1.6	1.4	0.7	0.9	0.9	0.5	0.8
Zr	108.9	133.6	139.5	126.6	131.8	195.6	225.6	215.8	188.6	159.0	120.2	217.1	189.1	103.7	172.1
Hf	2.8	3.5	3.6	3.1	3.3	4.8	6.0	5.1	4.7	4.0	3.2	5.2	4.6	2.5	4.4
Th	1.4	1.7	1.8	1.6	1.7	2.6	5.8	2.3	3.3	3.1	1.6	2.4	2.1	1.2	2.2
U	0.3	0.5	0.5	0.3	0.4	0.6	1.4	0.6	0.8	0.6	0.4	0.6	0.5	0.4	0.5

Table 1 (Contd.)

									Upper Unit Subunit1						
	CH02-17	CH02-18	CH02-19	CH02-20	CH02-21	CH02-22	CH02-24	CH02-25	CH02-26	CH02-27	CH02-29	CH02-30	CH02-31	CH02-32	CH02-33
Oxides (wt%)															
SiO_2	51.1	47.2	53.1	55.4	49.1	59.4	61.1	61.0	51.5	50.6	47.1	45.8	45.8	48.9	51.5
TiO_2	2.17	2.52	2.04	2.59	1.81	1.73	1.68	1.70	2.36	2.69	3.24	2.92	2.92	2.67	2.75
Al_2O_3	12.0	13.9	14.1	13.1	13.5	13.3	12.5	12.8	13.8	13.1	13.7	13.8	13.6	13. 7	13.2
Fe_2O_3	13.3	14.7	10.9	12.0	14.9	9.0	8.7	8.8	12.7	11.9	15.5	16.0	15.7	14.5	12.5
MnO	0.18	0.22	0.17	0.18	0.19	0.13	0.13	0.13	0.18	0.19	0.23	0.25	0.23	0.20	0.17
MgO	8.32	5.81	5.31	3.81	6.39	3.99	3.62	3.64	5.58	5.94	5.71	6.51	6.30	5.45	6.04
CaO	7.88	10.89	8.43	6.96	8.16	4.86	5.73	5.56	7.31	10.34	9.49	9.84	10.64	10.06	8.98
Na_2O	2.46	3.12	3.13	3.00	3.37	3.85	3.06	3.02	3.80	2.78	3.12	2.00	2.56	2.07	2.15
K_2O	1.11	0.57	1.24	1.47	1.30	2.15	1.60	1.85	1.12	0.77	0.78	1.42	0.88	1.21	1.51
P_2O_5	0.26	0.35	0.24	0.35	0.22	0.24	0.24	0.24	0.28	0.30	0.53	0.37	0.37	0.36	0.31
LOI	0.62	0.55	0.92	0.46	0.68	0.49	0.58	0.69	0.73	0.86	0.17	0.97	0.54	0.64	0.63
Total	99.42	99.81	99.60	99.33	99.54	99.06	98.97	99.45	99.38	99.51	99.64	99.88	99.60	99.70	99.71
Trace elements (ppm)															
Sc	29.3	30.6	26.8	22.7	42.3	22.9	22.1	20.9	28.0	27.0	29.2	30.2	32.7	29.8	27.8
V	339	402	300	327	393	253	242	236	405	385	409	465	467	451	335
Cr	60	37	18	3	37	20	8	19	−4	46	95	23	22	7	64
Co	57.5	50.1	40.0	37.4	63.8	27.6	28.4	31.2	43.0	41.6	55.6	63.1	49.0	54.9	52.2
Ni	77	44	39	6	58	24	25	22	32	64	70	54	47	52	77
Cu	240	86	78	17	142	58	62	42	58	48	218	169	20	101	144
La	22.0	25.8	24.1	33.5	16.8	35.5	30.9	32.1	25.0	28.7	26.4	31.1	32.3	29.5	29.0
Ce	45.9	56.4	50.7	70.6	34.1	69.9	64.4	66.5	52.4	62.9	56.7	66.0	66.2	61.6	63.7
Pr	6.3	7.7	6.9	9.6	4.5	9.0	8.6	8.8	7.2	8.7	7.9	8.7	8.7	8.1	8.7
Nd	27.5	33.1	29.7	40.7	19.8	37.0	35.4	36.3	31.6	37.9	34.9	36.9	37.0	34.6	38.2
Sm	6.0	6.8	6.4	8.7	4.7	7.6	7.5	7.6	6.8	8.0	7.6	7.9	7.8	7.4	8.0
Eu	1.9	2.3	2.0	2.5	1.6	2.0	1.9	2.0	2.3	2.5	2.7	2.6	2.6	2.4	2.4
Gd	5.4	6.1	5.8	7.8	5.0	6.7	6.6	6.6	6.1	6.9	6.7	7.1	7.1	6.6	6.8
Tb	0.8	1.0	0.9	1.2	0.9	1.1	1.1	1.1	1.0	1.1	1.1	1.1	1.1	1.1	1.1
Dy	4.9	5.6	5.4	7.2	5.9	6.4	6.3	6.4	5.5	5.8	6.1	6.4	6.5	6.1	5.8
Ho	1.0	1.1	1.1	1.4	1.3	1.3	1.3	1.3	1.1	1.1	1.2	1.2	1.3	1.2	1.1
Er	2.6	2.9	2.9	3.7	3.6	3.6	3.6	3.5	2.8	2.8	3.1	3.3	3.4	3.1	2.8
Tm	0.3	0.4	0.4	0.5	0.5	0.5	0.5	0.5	0.3	0.4	0.4	0.4	0.4	0.4	0.3
Yb	2.2	2.4	2.5	3.2	3.2	3.4	3.2	3.2	2.3	2.3	2.5	2.7	2.8	2.6	2.2
Lu	0.3	0.3	0.4	0.5	0.5	0.5	0.5	0.5	0.3	0.3	0.4	0.4	0.4	0.4	0.3
Rb	27.0	6.1	31.8	37.5	31.1	49.3	46.6	53.5	20.6	12.0	13.0	35.6	21.9	25.5	45.1
Sr	137.5	471.1	395.7	221.2	109.5	378.6	305.1	305.7	127.1	382.2	451.2	427.9	405.8	473.8	546.0
Ba	254.6	127.8	533.3	477.7	243.6	620.4	621.3	694.6	306.8	286.9	362.6	425.0	287.1	336.4	637.4
Y	24.6	27.6	27.5	36.3	33.0	34.6	34.1	33.7	26.5	27.4	29.5	32.0	33.0	30.5	27.3
Nb	13.6	23.2	14.4	19.2	16.0	15.8	15.1	15.7	14.7	23.3	22.0	25.8	29.3	24.6	22.4
Ta	0.8	1.4	0.9	1.2	0.9	1.0	1.0	1.0	0.9	1.4	1.4	1.6	1.7	1.5	1.4
Zr	187.0	166.4	200.8	266.7	122.0	230.9	223.3	212.9	199.6	217.3	153.8	225.5	221.7	220.3	221.1
Hf	4.6	4.1	5.0	6.7	3.2	6.0	5.7	5.6	4.9	5.5	3.9	5.5	5.4	5.4	5.4
Th	2.3	2.9	3.3	4.6	2.5	6.1	5.9	6.0	2.4	3.7	2.8	4.4	4.5	4.2	3.7
U	0.6	0.7	0.8	1.1	0.6	1.4	1.3	1.3	0.6	1.0	0.7	1.1	1.1	1.3	1.1

Table 1 (Contd.)

		Subunit 2						Subunit 3					
	CH02-34	CH02-35	CH02-36	CH02-37	CH02-38	CH02-39	CH02-40	CH02-41	CH02-42	CH02-43	CH02-44	CH02-45	CH02-46
Oxides (wt%)													
SiO_2	42.7	47.6	48.7	50.1	48.5	47.9	46.5	48.7	49.1	46.0	46.3	50.1	46.7
TiO_2	3.36	1.69	1.84	1.74	1.80	2.77	1.89	2.78	2.75	1.91	1.94	1.81	1.93
Al_2O_3	14.1	13.7	14.3	13.4	13.0	13.4	13.6	12.8	13.6	14.6	14.5	14.0	14.6
Fe_2O_3	17.2	15.4	13.5	13.7	15.0	14.5	16.1	14. 6	14.4	13.9	14.0	12.8	14.8
MnO	0.26	0.23	0.25	0.21	0.16	0.20	0.23	0.22	0.22	0.22	0.22	0.20	0.22
MgO	6.71	6.65	7.46	6.20	6.97	5.91	6.99	5.92	5.61	7.49	7.59	6.55	7.05
CaO	10.43	11.18	9.35	10.03	9.24	9.46	9.49	10.55	10.21	11.68	11.71	10.58	11.32
Na_2O	2.12	2.12	3.22	2.84	3.18	3.23	3.01	2.65	2.40	2.21	2.11	2.34	2.09
K_2O	1.36	0.52	0.56	0.78	1.10	0.84	0.95	0.53	0.42	0.36	0.36	0.34	0.39
P_2O_5	0.42	0.23	0.25	0.22	0.23	0.43	0.23	0.41	0.43	0.19	0.19	0.18	0.18
LOI	1.02	0.49	0.36	0.76	0.66	1.00	0.62	0.66	0.46	0.84	0.73	0.75	0.67
Total	99.64	99.82	99.77	99.94	99.88	99.67	99.56	99.81	99.66	99.40	99.59	99.63	99.97
Trace elements (ppm)													
Sc	37.7	43.3	42.4	41.5	41.1	31.2	43.2	28.0	31.9	33.9	32.6	30.5	32.8
V	496	377	387	375	400	414	402	405	408	382	382	355	389
Cr	4	144	35	45	47	33	48	92	34	204	177	108	116
Co	58.1	64.4	57.7	57.4	64.2	56.0	66.3	49.7	51.8	59.9	61.0	51.4	50.2
Ni	61	81	50	56	63	49	58	66	41	95	100	79	72
Cu	75	184	212	146	262	190	272	65	120	96	90	56	57
La	37.4	14.9	15.1	16.4	14.8	27.4	15.7	22.8	28.0	13.0	13.4	13.5	13.3
Ce	77.7	30.6	32.9	33.1	31.4	57.7	33.5	48.7	58.8	29.3	29.6	30.2	29.8
Pr	10.4	4.1	4.5	4.4	4.2	8.0	4.6	6.8	8.0	4.2	4.3	4.3	4.3
Nd	43.3	17.6	19.4	18.7	18.4	34.5	19.8	30.0	34.3	19.2	19.4	19.7	20.1
Sm	9.3	4.1	4.6	4.5	4.5	7.2	4.8	6.3	7.0	4.8	4.7	4.9	4.8
Eu	2.8	1.4	1.3	1.4	1.4	2.5	1.6	2.1	2.5	1.8	1.7	1.7	1.7
Gd	8.3	4.4	4.8	4.8	4.6	6.4	5.1	5.7	6.4	4.7	4.7	4.6	4.7
Tb	1.4	0.8	0.9	0.9	0.8	1.0	0.9	0.9	1.0	0.8	0.8	0.8	0.8
Dy	7.7	5.4	5.6	5.6	5.5	5.7	6.1	5.0	5.7	4.8	4.7	4.7	4.7
Ho	1.5	1.2	1.2	1.2	1.2	1.1	1.3	1.0	1.1	0.9	0.9	0.9	0.9
Er	3.9	3.4	3.3	3.4	3.3	3.0	3.6	2.6	3.0	2.4	2.5	2.4	2.5
Tm	0.5	0.5	0.4	0.5	0.5	0.4	0.5	0.3	0.4	0.3	0.3	0.3	0.3
Yb	3.2	3.1	3.0	3.1	3.1	2.4	3.2	2.1	2.4	2.1	2.0	2.0	2.1
Lu	0.5	0.5	0.4	0.5	0.5	0.4	0.5	0.3	0.4	0.3	0.3	0.3	0.3
Rb	38.3	5.1	7.6	13.9	23.5	14.7	21.1	5.6	2.4	1.4	1.4	2.6	2.2
Sr	381.9	268.2	274.3	321.0	92.8	335.1	133.6	410.3	369.1	245.0	233.4	252.3	207.1
Ba	395.2	74.1	164.6	139.0	135.8	308.1	202.6	170.7	83.9	46.4	48.4	92.2	62.2
Y	37.5	31.5	30.7	32.1	30.5	28.7	33.6	25.9	28.7	24.8	24.8	24.3	24.6
Nb	30.7	15.8	16.7	16.3	17.1	22.2	12.7	21.4	22.3	12.1	12.6	14.4	10.5
Ta	1.8	0.9	0.9	0.9	0.9	1.4	0.7	1.1	1.3	0.7	0.7	0.7	0.6
Zr	266.6	98.7	115.5	103.7	110.3	162.6	127.0	126.9	160.0	120.0	110.6	111.1	125.4
Hf	6.5	2.5	2.9	2.6	2.9	3.9	3.2	3.0	3.8	3.0	2.8	2.8	3.2
Th	5.4	1.7	2.5	2.4	2.4	2.8	2.6	2.3	2.8	1.6	1.7	1.6	1.6
U	1.3	0.4	0.9	0.8	0.5	0.7	0.5	0.5	0.7	0.4	0.4	0.4	0.4

Table 2 Concentrations of platinum-group elements in the Yangliuping basalts

	Au (ppb)	Ir (ppb)	Ru (ppb)	Rh (ppb)	Pd (ppb)	Pt (ppb)
Detection limit	0.71	0.04	0.13	0.08	0.11	0.14
Lower Unit						
CH02-2	4.61	0.11	0.23	0.38	11.54	13.65
CH02-3	1.75	0.06	0.16	0.37	10.8	9.44
CH02-4	N.D.	0.08	0.2	0.41	12.78	11.47
CH02-5	N.D.	0.08	0.24	0.38	5.33	9
CH02-6	2.47	0.08	0.2	0.36	11.36	10.76
CH02-7	N.D.	0.15	N.D.	N.D.	2.4	6.59
CH02-8	N.D.	N.D.	N.D.	N.D.	0.36	0.29
Middle Unit						
CH02-9	N.D.	N.D.	N.D.	N.D.	0.14	0.15
CH02-10	N.D.	0.2	N.D.	0.46	10.54	11.94
CH02-11	0.93	0.18	N.D.	0.42	7.46	11.14
CH02-12	N.D.	0.1	0.19	0.41	10.81	10.86
CH02-13	N.D.	N.D.	N.D.	N.D.	N.D.	0.15
CH02-14*		0.09	0.17	0.04	0.75	1.04
CH02-15	1.11	N.D.	N.D.	N.D.	0.28	0.46
CH02-16	2.84	0.14	N.D.	N.D.	2.04	3.53
CH02-17	4.56	0.09	N.D.	N.D.	0.88	2.24
CH02-18	0.84	0.18	0.17	0.39	7.46	9.76
CH02-19	N.D.	N.D.	N.D.	N.D.	N.D.	N.D.
CH02-20	N.D.	N.D.	N.D.	N.D.	N.D.	N.D.
CH02-21	4.16	N.D.	0.15	0.58	13.61	10.7
CH02-22	N.D.	N.D.	N.D.	N.D.	0.14	0.26
CH02-24	N.D.	N.D.	N.D.	N.D.	N.D.	0.28
CH02-25	N.D.	N.D.	N.D.	N.D.	0.13	0.24
Upper Unit						
Subunit 1						
CH02-26	N.D.	N.D.	N.D.	N.D.	N.D.	N.D.
CH02-27	N.D.	0.24	0.18	0.28	7.68	14.49
CH02-29	2.45	0.2	0.14	0.31	8.42	8.52
CH02-30	N.D.	0.14	N.D.	0.24	5.35	10.55
CH02-31	N.D.	0.13	N.D.	0.33	7.43	9.83
CH02-32*		0.19	0.21	0.18	11.46	8.69
CH02-33	0.82	0.22	0.32	0.27	10.31	16.72
CH02-34	N.D.	0.16	0.13	0.3	6.11	13.06
Subunit 2						
CH02-35*		0.17	0.16	0.50	12.35	18.89
CH02-36	1.23	N.D.	0.15	0.56	17.76	11.41
CH02-37	5.98	N.D.	0.14	0.58	18.66	11.41
CH02-38	13.56	N.D.	0.16	0.62	18.62	11.04
CH02-39	2.42	0.17	0.16	0.39	8.75	10.73
CH02-40	9.39	N.D.	0.18	0.58	26.88	12.01
Subunit 3						
CH02-41	0.94	0.14	N.D.	0.29	6.96	7.91
CH02-42	N.D.	0.14	N.D.	0.4	9.36	10.09
CH02-43	N.D.	0.11	0.26	0.47	10.18	12.53
CH02-44	N.D.	0.1	0.3	0.42	10.15	11.83
CH02-45	N.D.	0.07	0.25	0.39	10.77	11.37
CH02-46	N.D.	0.07	0.22	0.35	7.99	8.11

Sample signed by (*) were analyzed at Department of Earth Sciences in The University of Hong Kong

Lower Unit

With only a few exceptions, the Lower Unit basalts exhibit a narrow range of chemical variations: 48.5–50.0 wt% SiO_2, 6.0–7.0 wt% MgO, and 57–80 ppm Ni (Fig. 4). The basalts have 1.5–2.1 wt% TiO_2, and high Ti/Y ratios (450–550). Ratios of La/Sm (2.5–3.5) and Gd/Yb (2.2–2.4) are constant, and the chondrite-normalized REE patterns are relatively LREE enriched (Fig. 5a). The basalts of the Lower Unit have medium Zr/Nb ratios (10–z12) and contain 9.0–13.6 ppb Pt, 5.3–12.8 ppb Pd, 0.08–0.11 ppb Ir, 0.2–0.24 ppb Ru, and 0.36–0.41 ppb Rh, with exception of the two samples with more than 50 wt% SiO_2 at the top of this Unit (Table 3; Fig. 4).

Primitive mantle normalized trace element patterns show that the basalts are enriched in HFSEs and have very weakly negative Nb- and Ta-anomalies, whereas sample CH02-8 with 61.4 wt% SiO_2 has strongly negative Nb- and Ta-anomalies and positive Zr- and Hf-anomalies (Fig. 6a).

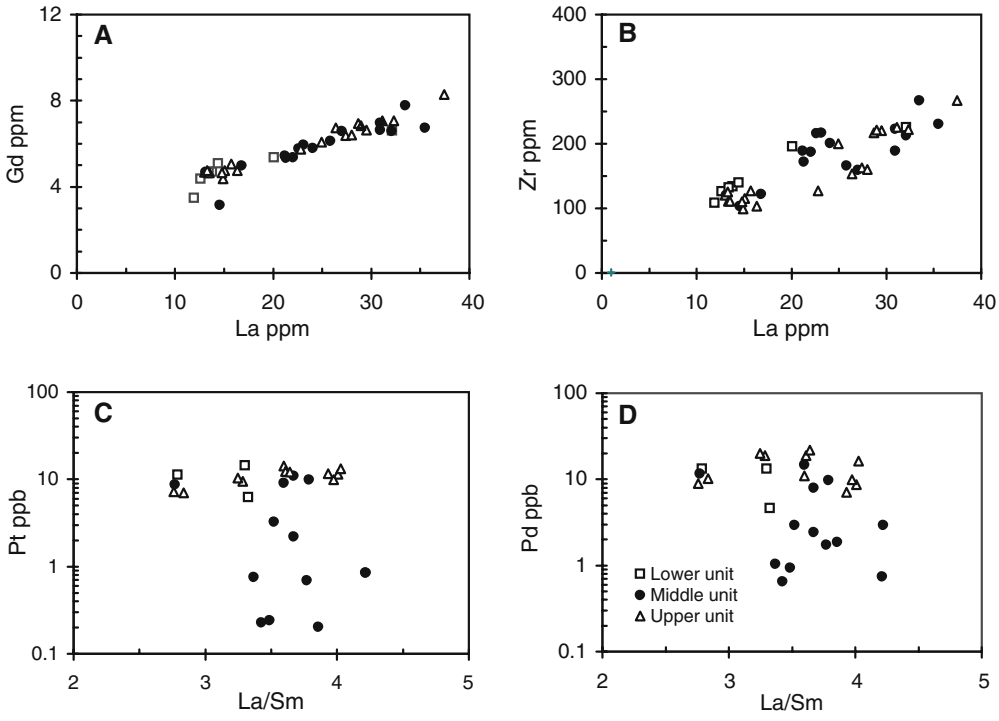

Fig. 3 Scattergrams of **a** Gd vs La, **b** Zr vs La, **c** Pt vs La/Sm, and **d** Pd vs La/Sm for the Yangliuping basalts

Middle Unit

The Middle Unit shows large compositional variations. Silica contents increase from about 47 wt% at the base to 61 wt% at the top, TiO_2 decreases from 2.8 to 1.7 wt%, and MgO ranges from 3.8 to 8.3 wt%. Most samples have 20–92 ppm Ni (Fig. 4). The Middle Unit has a wide range of REE concentrations, e.g., 13–35.5 ppm La, 28–71 ppm Ce, and 1.5–3.5 ppm Yb, and LREE-enriched chondrite-normalized REE patterns (Table 1; Fig. 5b). The Gd/Yb ratios mostly range from 2.0 to 2.7, similar or slightly higher than those of the Lower Unit, except for CH02-8, which has high SiO_2, at the top of this Unit. The Ti/Y (mostly $\sim$ 400–600) ratios are similar to those of the Lower Unit, whereas the La/Sm ratios (mostly >3.0) are obviously higher than those of the Lower Unit (Fig. 4). The Zr/Nb ratios of the Middle Unit are extremely variable, varying from <6.0 to 14.5 (Fig. 4; Table 1).

Many samples of the Middle Unit are strongly PGE-depleted with some samples having PGE abundances lower than the detection limits (Table 3; Fig. 4). These samples have high Zr/Nb ratios (up to 14.5), extensive negative Nb- and Ta-anomalies (Fig. 6b), and low $\varepsilon_{Nd(260\ Ma)}$ values (<2.5) (Fig. 4). In contrast, the lavas with normal PGE abundances (>8 ppb) have low Zr/Nb (<8) and high $\varepsilon_{Nd(260\ Ma)}$ values (>2.5) (Fig. 4).

Upper Unit

The Upper Unit is subdivided into three subunits based on Ti/Y and Gd/Yb ratios (Figs. 4, 6). Subunit 1, at the base, is distinct from the Middle Unit by obviously elevated TiO_2 (mostly >2.5 wt%) and Ti/Y ratios (>500). Primitive mantle normalized trace element patterns show that Subunit 1 has the weakest negative Nb- and Ta-anomalies of all the units (Fig. 6c). This subunit has moderate PGE concentrations (e.g., 8.5–14.5 ppb Pt and 5.4–11.5 ppb Pd), except for CH02-26, which has PGE abundances lower than the detection limits (Table 3; Fig. 4).

Subunit 2 is distinctive from other units by low Gd/Yb values (<2.0, except for CH02-39) and Ti/Y ratios (<400, except for CH02-39) (Fig. 4), with MREE–HREE flat chondrite-normalized REE patterns (Fig. 5d). Abundances of the PGE in five of the six Subunit 2 samples (11.0–18.9 ppb Pt and 12.8–26.9 ppb Pd) are significantly higher than those of Subunit 1 (Table 3; Fig. 4); the remaining Subunit 2 sample has 10.7 ppb Pt and 8.8 ppb Pd. The primitive mantle normalized trace element patterns are relatively flat without Nb–Ta and Zr–Hf anomalies except for one sample (Fig. 6d).

Subunit 3 has elevated Gd/Yb (>2.0) and Ti/Y ratios (>400) and lower La/Sm ratios, and generally slightly lower PGE abundances (e.g., 7.9–12.5 ppb Pt and 7.0–10.8 ppb Pd) than Subunit 2 (Table 3; Fig. 4).

Discussion

Changes in the depth of partial melting

Both Yb and Y have high garnet/melt partition coefficients, whereas Ti and Gd have low garnet/melt partition coefficients (Rollinson 1993). Hence, high Gd/Yb

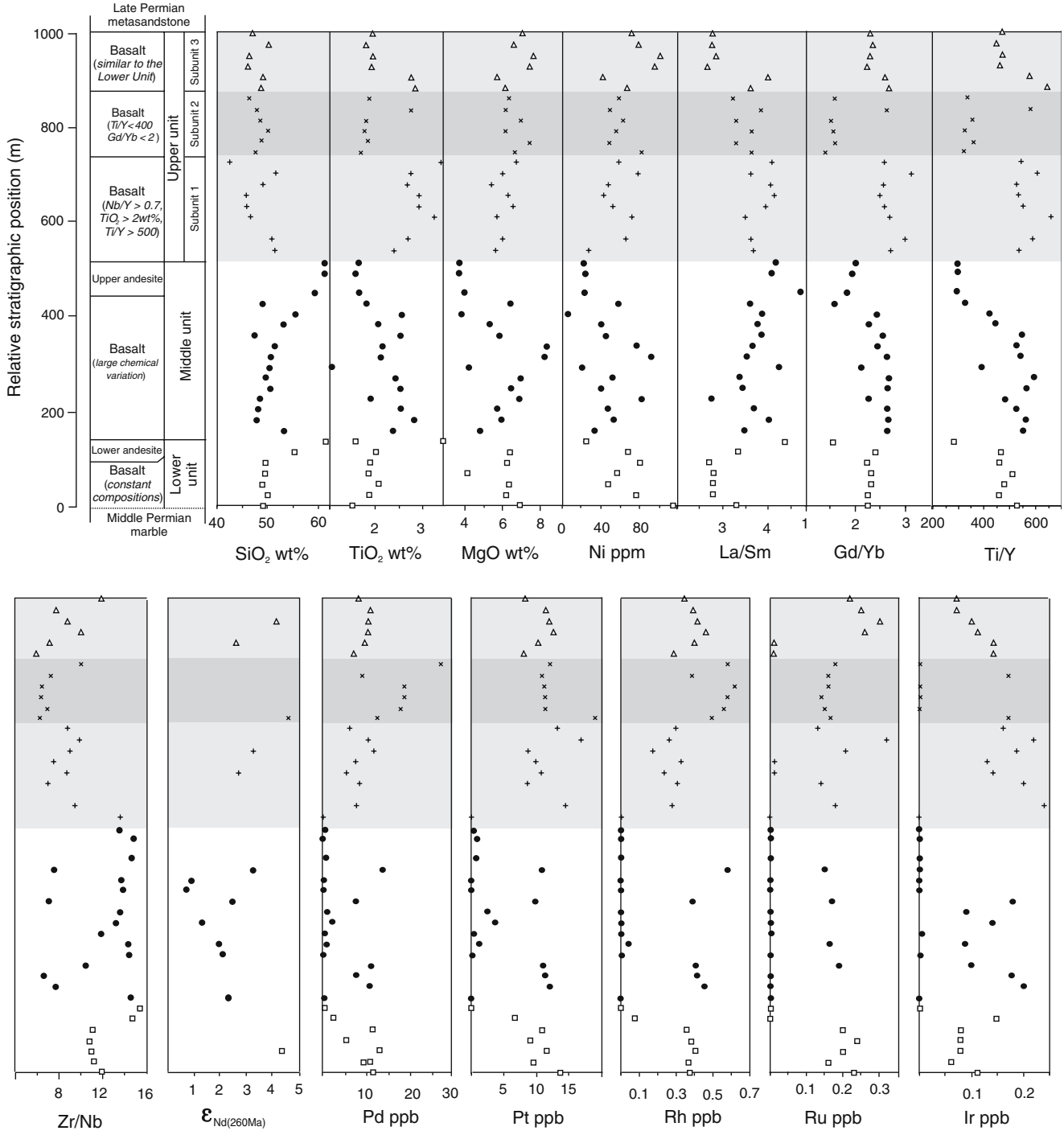

Fig. 4 Chemostratigraphic columns of the Yangliuping basalts in the northern margin of the Yangliuping dome. Many samples of the Middle Unit have very low PGE concentrations; those samples with PGE contents lower than the detection limits are plotted along the *y*-axes

and Ti/Y ratios can be used to determine whether or not garnet was involved in the petrogenesis of the rocks. Most of the Yangliuping basalts have Ti/Y > 400, Gd/Yb > 2.0, and Sc contents < 35 ppm (Fig. 7). However, the basalts of Subunit 2 of the Upper Unit have low Gd/Yb (< 2.0) and Ti/Y (< 400) and high Sc contents (> 35 ppm) (Fig. 7). There is no petrographic evidence of garnet as a crystallized phase in the lavas or related mafic–ultramafic intrusions in the Yangliuping area. Thus, the high Gd/Yb ratios of all of the Yangliuping basaltic samples except those of Subunit 2 imply that the parental magmas of these basalts were derived from a mantle source in which garnet was a stable phase. Since there is no evidence of mixing between

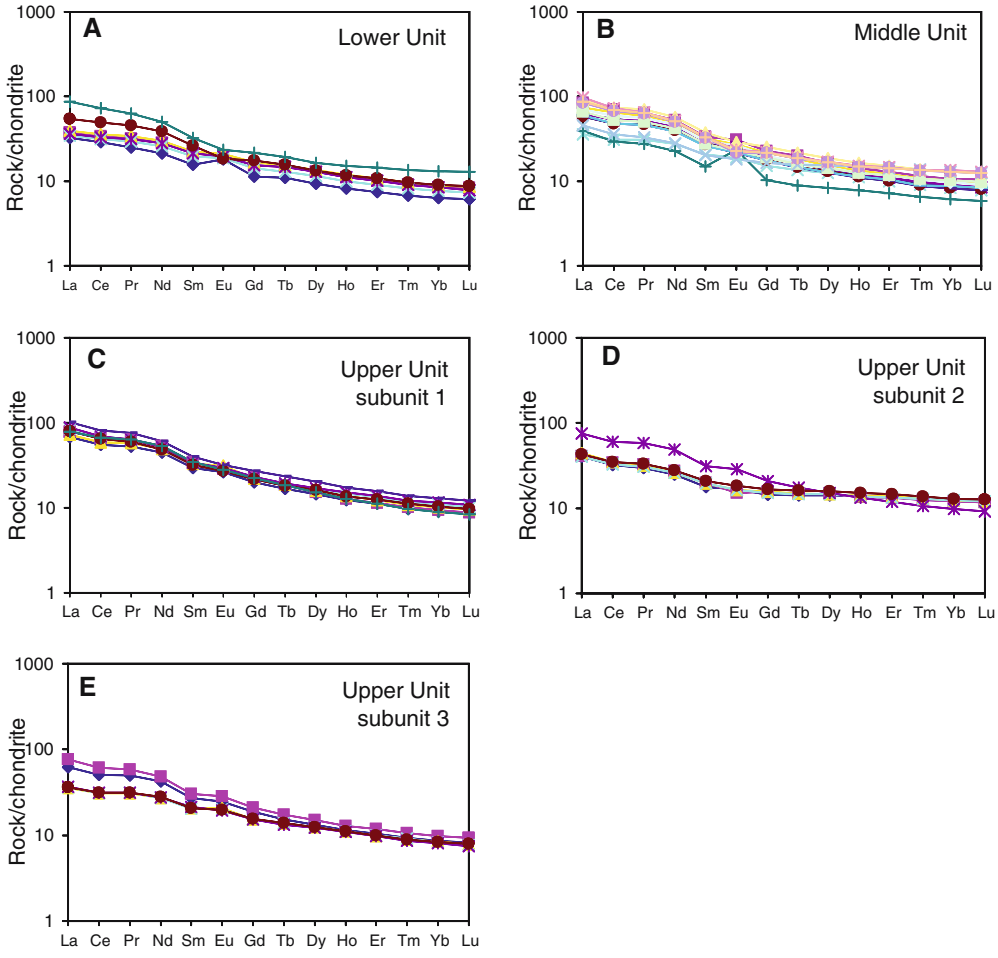

Fig. 5 Chondrite-normalized rare earth elements patterns of the Yangliuping basalts. **a** Lower Unit, **b** Middle Unit basalts, **c** Subunit 1 basalts of the Upper Unit, **d** Subunit 2 basalts of the Upper Unit, and **e** Subunit 3 of the Upper Unit. Chondrite values are from Taylor and McLennan (1985)

Table 3 Nd isotopic compositions of intrusive and extrusive rocks

Sample no.	$^{143}Nd/^{144}Nd$	2 *Err.*	Nd (ppm)	Sm (ppm)	$^{147}Sm/^{144}Nd$	$\varepsilon_{Nd(260\ Ma)}$
Lower Unit						
CH02-4	0.512776	0.000010	21.28	5.16	0.146776	4.35
Middle Unit						
CH02-9	0.512643	0.000009	30.19	6.48	0.129839	2.33
CH02-13	0.512637	0.000010	30.63	6.75	0.133187	2.10
CH02-14	0.512631	0.000009	28.39	6.30	0.13403	1.95
CH02-16	0.512597	0.000010	27.43	6.05	0.133212	1.31
CH02-18	0.512643	0.000010	33.07	6.82	0.12459	2.49
CH02-19	0.512558	0.000009	29.66	6.38	0.130077	0.65
CH02-20	0.512564	0.000009	40.65	8.68	0.129095	0.81
CH02-21	0.512711	0.000011	19.78	4.67	0.142688	3.22
Upper Unit						
Subunit 1						
CH02-30	0.512660	0.000014	36.93	7.91	0.129505	2.66
CH02-32	0.512692	0.000010	34.58	7.36	0.128721	3.31
Subunit 2						
CH02-35	0.512785	0.000009	17.60	4.12	0.141624	4.70
CH02-38	0.512721	0.000010	18.40	4.50	0.147355	3.27
Subunit 3						
CH02-42	0.512653	0.000009	34.32	7.05	0.124076	2.70
CH02-44	0.512766	0.000010	19.42	4.71	0.146711	4.17

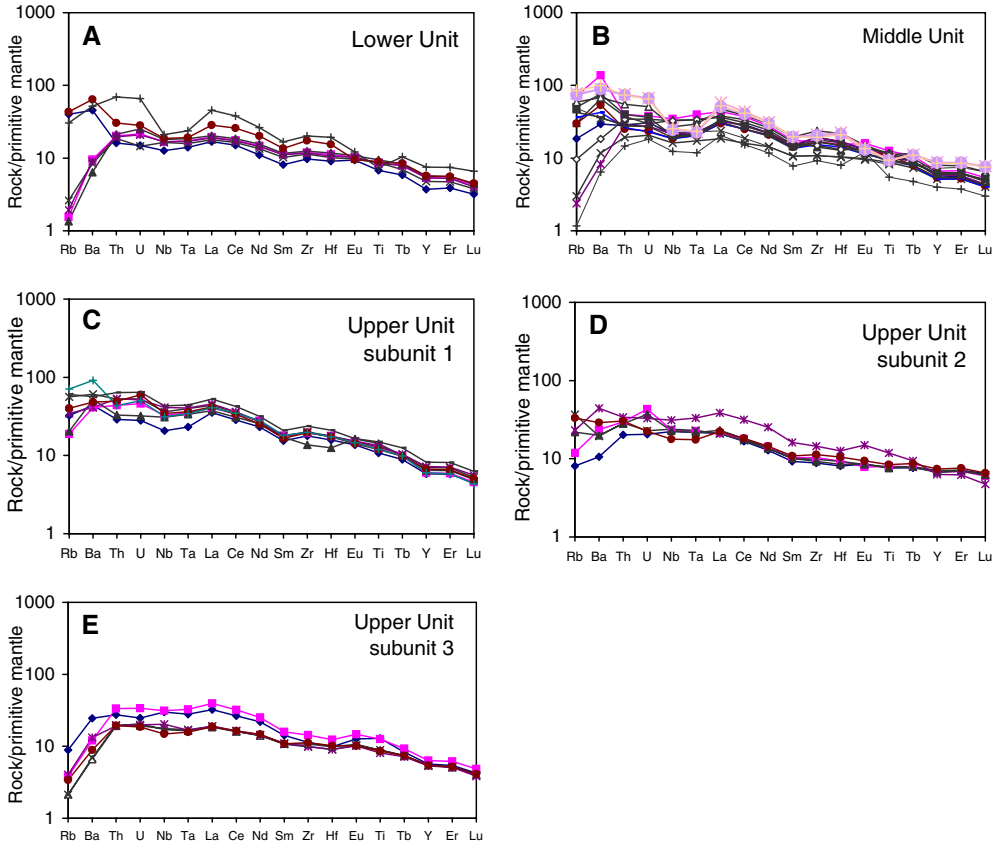

Fig. 6 Primitive mantle normalized trace element patterns of the Yangliuping basalts from Yangliuping cross-section. **a** Lower Unit, **b** Middle Unit, **c** Subunit 1 of the Upper Unit, **d** Subunit 2 of the Upper Unit, **e** Subunit 3 of the Upper Unit. Primitive mantle values are from Hofmann (1988)

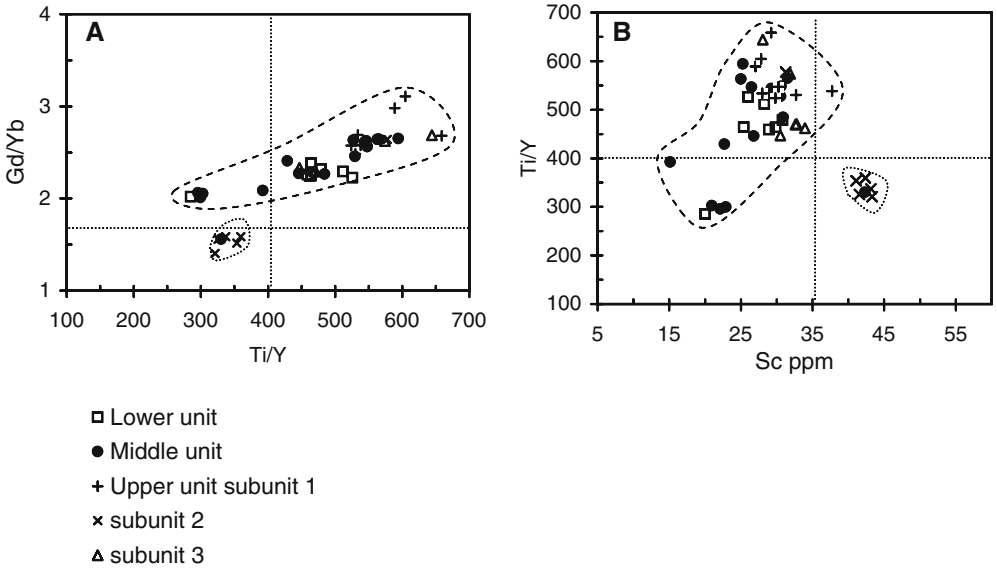

Fig. 7 Scattergrams showing the chemical diversities of basalts from the different units: **a** Gd/Yb against Ti/Y and **b** Ti/Y against Sc

Subunit 2 and Subunits 1 and 3 (e.g., Gd/Yb and Ti/Y), the low Gd/Yb ratios of the Subunit 2 basalts suggest that these lavas formed in a distinct spinel-bearing mantle at a shallower depth synchronously with the enveloping basalts and fed by their own coexisting but isolated feeder system. Similarly, high-Ti and low-Ti Paleogene flood basalts in East Greenland were generated by two melting regimes (Momme et al. 2005).

Fractional crystallization

The presence of plagioclase phenocrysts in the Yangliuping basalts suggests that the magmas experienced extensive crystallization before eruption. However, alteration and metamorphism of the lavas and their relatively small compositional variations make it difficult to establish the crystallization sequence of the basalts.

Field relationships indicate that the Permian basalts are temporally related to the mafic–ultramafic intrusions in the Yangliuping region (Song et al. 2003). Coherent compositional variations of the intrusive and extrusive rocks indicate that they are genetically linked, and that the intrusions comprise cumulates deposited by the magmas that erupted to form some of the lavas (Fig. 8a–f). The lithological zones, cumulus textures, and chemical variations in the Yangliuping and Zhengaiyanwuo sills indicate that the chemical variations of the intrusive and extrusive rocks were mainly controlled by mafic minerals (Song et al. 2003). The small proportion of gabbro in the sills and the presence of plagioclase phenocrysts in the basalts indicate that plagioclase was the latest phase to crystallize.

Both Cr and Sc are incompatible in olivine, but compatible in pyroxene, and Cr is strongly compatible in chromite (Arth 1976; Fujimaki et al. 1984; Hawkesworth et al. 1995). Thus, the positive correlations between Ni, Cr, and MgO (Fig. 8d, e) and negative correlation between Sc and MgO for samples from sulfide-bearing sills, which have MgO > 10 wt% (Fig. 8f), indicate that chromite and olivine were the main early crystallizing phases. The sharp decreases in CaO and Sc (without a decrease in Al_2O_3) with decreasing MgO for samples with less than 10 wt% MgO suggest that clinopyroxene crystallization followed olivine + chromite (Fig. 8a, b, f). Decrease of TiO_2 with decreasing MgO in the basalts indicates that oxides (probably magnetite + ilmenite) crystallized in the latest stages of fractionation (Fig. 8c).

Thus, we conclude that the crystallization sequence was olivine + chromite → pyroxene (mainly clinopyroxene) → plagioclase + oxides.

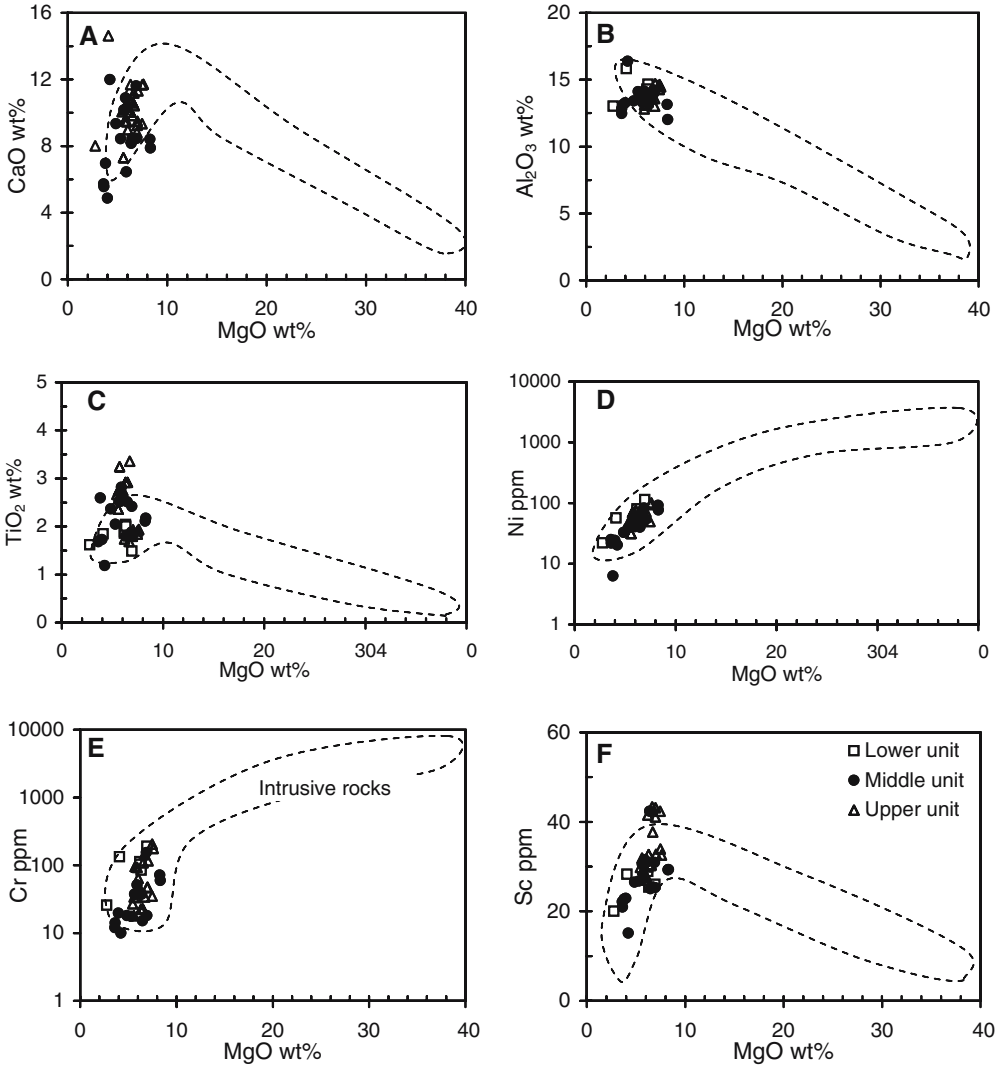

Fig. 8 Plots of oxides and transition elements vs MgO of the volcanic rocks and intrusive rocks of the sulfide-bearing sills in the Yangliuping region. The plotting areas of the intrusive rocks are shown by *dashed lines*

Ratios of strongly incompatible elements are constant, and typically do not change during fractional crystallization. The intrusive rocks of the Yangliuping and Zhengziyanwuo sills overlap with most samples of the Middle Unit on the diagrams of Gd/Yb vs La/Sm and Th/Yb vs Gd/Yb (Fig. 9a, b). In addition, the intrusive rocks have Nd isotope values overlapping but slightly lower than those of the Middle Unit, although their Nb/La values are slightly higher, probably because of the presence of oxides, such as ilmenite (Fig. 10a). Experiments indicate that the ilmenite/silicate liquid partition coefficients of Nb and Ta are much higher than 1.0 (Green and Pearson 1986), whereas that of La is less than 0.01 (Nielson et al. 1992). Thus, the similar $\varepsilon_{Nd(260\ Ma)}$ values indicate a close genetic link between the Middle Unit and the mineralized intrusions (Fig. 10a).

The Pd/Pt ratios of the PGE-undepleted Yangliuping basalts range from 0.47, which is close to the average Pd/Pt ratio (0.57) of the mantle (Taylor and McLennan 1985), up to 2.3 (Fig. 11). This range in Pd/Pt ratios together with the range in Pd and Pt values of the Yangliuping basalts is very similar to that reported for the PGE-undepleted basalts of the Siberian Traps basalts by Lightfoot and Keays (2005). Because the Pd contents of the PGE-undepleted Siberian Traps basalts increase with increasing amounts of incompatible lithophile elements such as Zr, but Pt contents remain constant, Lightfoot and Keays (2005) attributed this to fractionation of S-undersaturated magmas which produced the PGE-undepleted basalts. Hence, the least fractionated Siberian Traps basalts have Pd/Pt ratios close to mantle ratios whereas the most fractionated basalts have the highest Pd/Pt ratios.

In the PGE-undepleted Yangliuping basalts (Pd > 4 ppb and Pt > 4 ppb) (Fig. 11), the increase of Zr contents is possibly due to increasing amounts of fractionation and contamination, but Pt contents remain constant (Fig. 12a), just as they do in the PGE-undepleted lavas of the Siberian Traps (Lightfoot and Keays 2005). In contrast, Pd contents decrease with increasing Zr values (Fig. 12b); this is the opposite to what Lightfoot and Keays (2005) observed in the PGE-undepleted lavas of the Siberian Traps. The decrease in Pd values with increasing Zr values in the Yangliuping basalts indicates that the precursor magmas were mildly S-saturated and that they had segregated a small amount of sulfides.

The variations of Pd and Pt in the lavas due to fractional crystallization can be modeled using the Raleigh Fractionation law:

$$C_l = C_0 \times F^{(D-1)}$$

where C_1 is the concentration of element in silicate melt at a specified melt fraction (F) remaining, C_0 the initial

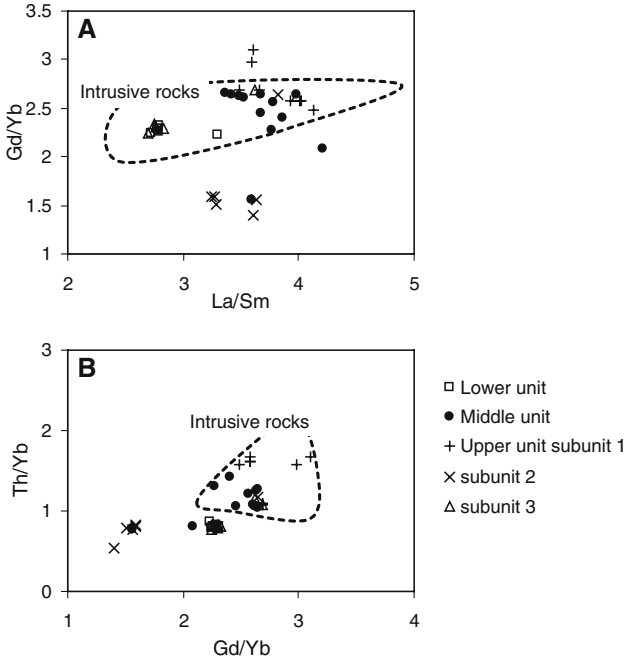

Fig. 9 Scattergrams comparing the chemical variations in the lavas with those of the intrusives. Relationships between the intrusive rocks and lavas shown by *diagrams* of **a** Gd/Yb vs La/Sm and **b** Th/Yb vs Gd/Yb. The fields for the intrusive rocks (outlined by the *dashed lines*) were constructed with data from X.-Y. Song (unpublished data)

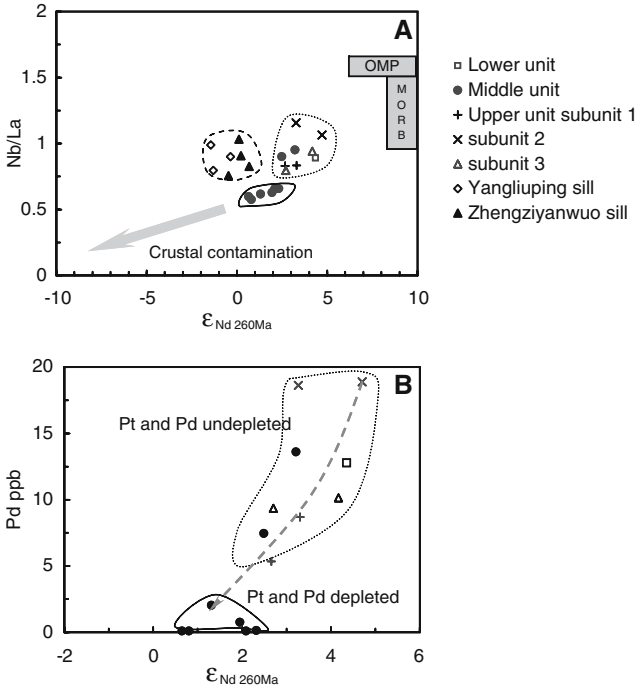

Fig. 10 **a** Nb/La vs $\varepsilon_{Nd(260\ Ma)}$ showing that the Middle Unit has ε_{Nd} values lower than those of the Lower and Upper Units and similar to those of the intrusive sills. Similar ε_{Nd} values suggest a genetic link between the Middle Unit and the intrusive rocks. The high Nb/La of the intrusive rocks is because the cumulates contain oxides. OPM means average oceanic plume magma (adopted from Gibson et al. 1996). **b** The Pd-depletion of the Middle Unit is correlated with a decrease in $\varepsilon_{Nd(260\ Ma)}$ values, the Pd concentrations less than the detection limit (0.14 ppb) are treated as 0.1 ppb in the diagram of Pd vs $\varepsilon_{Nd(260\ Ma)}$

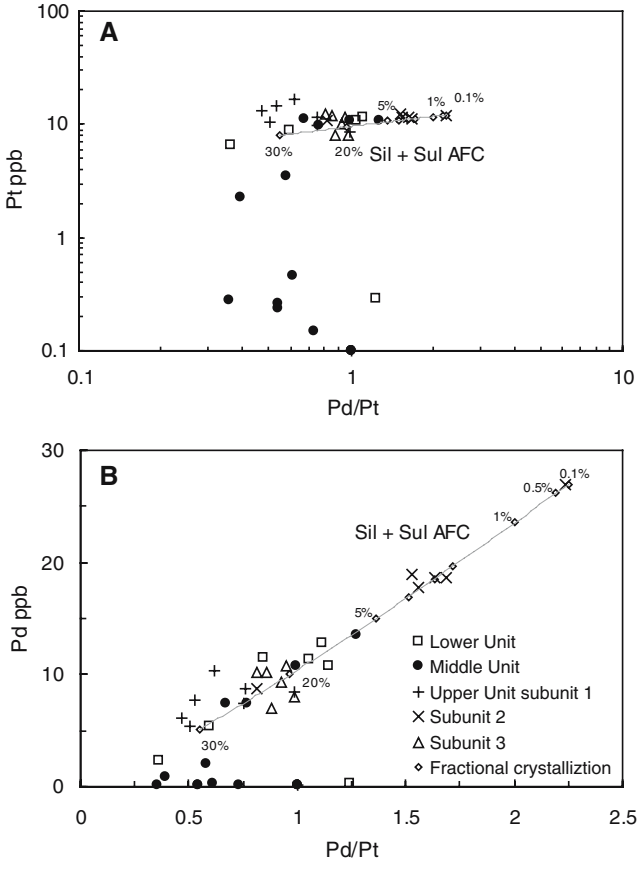

Fig. 11 Variation of **a** Pt vs Pd/Pt and **b** Pd vs Pd/Pt in the Yangliuping basalts. Samples that are strongly PGE-depleted underwent AFC processes that led to significant sulfide removal from the magmas. The remaining samples lie along the silicate + sulfide AFC fractionation curve (= *Sil + Sul AFC*) calculated for removal of 0.01% sulfide along with the silicate and oxide fractionating phases. The ticks along the curves give the degree of fractionation. The concentrations of Pt and Pd less than the detection limits are treated as 0.1 ppb in the plotting

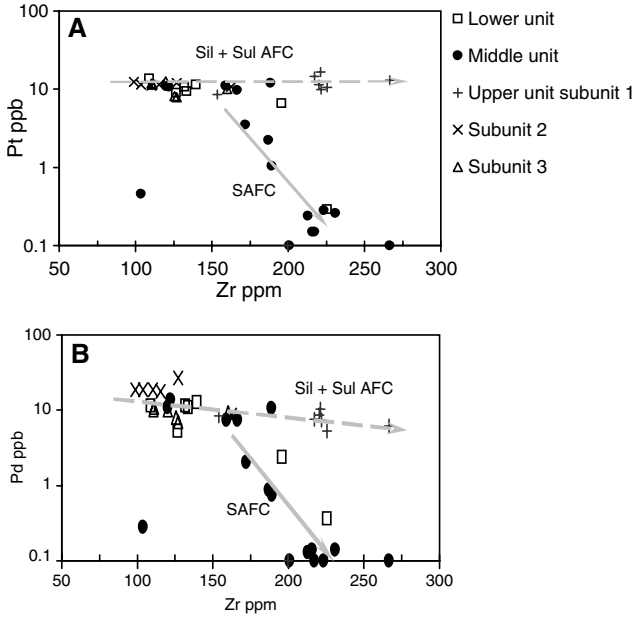

Fig. 12 Scattergrams of **a** Pt vs Zr and **b** Pd vs Zr. *Sil + Sul AFC* = AFC processes in which minor amounts (0.01%) of sulfides were removed along with the fractionating silicate and oxide phases; *SAFC* = AFC processes in which major amounts of magmatic sulfides were removed from the magma(s). The concentrations of Pt and Pd less than the detection limits are treated as 0.1 ppb in the plotting

concentration of the element in the silicate melt, F the fraction of melt remaining, and D the Nernst partition coefficient.

Modeling of the variations in Pd/Pt ratios due to fractionation has been done for the Subunit 2 basalts because these have the highest Pd and Pt contents and the lowest Zr contents; that is, they may be the least fractionated magma. The modeling was done assuming that the variations in Pd and Pt are due to fractionation and that the material fractionating from the basaltic magma was 0.01% sulfide melt and 99.99% silicate + oxide minerals. It was further assumed that the initial Pd and Pt contents were 27 and 12 ppb, respectively, sulfide/silicate melt partition coefficients were 35,000 and 7,000 for Pd and Pt, respectively, and silicate and oxide minerals/silicate melt partition coefficients were 0.5 and 0.75 for Pd and Pt, respectively.

The use of these assumptions permits an excellent fit to the data for the Subunit 2 basalts (Fig. 11). Although the other basalt suites are not comagmatic with the Subunit 2 basalts, the model curves for the Subunit 2 basalts provide a reasonable fit to the data for these suites as well (Fig. 11). The variation in the Pd/Pt ratios of the Subunit 2 basalts can be accounted for in terms of ~25% fractionation of the magma that produced these basalts.

Although some of the Middle Unit basalts plot along the fractionation path of the mildly PGE-depleted basalts, a number of them plot well below the fractionation path and have Pd and Pt contents considerably less than the mildly PGE-depleted basalts. The PGE-depleted basalts have Pd/Pt ratios that lie at the low end of the range of Pd/Pt ratios of the PGE-undepleted basalts (Fig. 11).

Crustal contamination

Crustal contamination plays a critical role in the formation of Ni–Cu–(PGE) sulfide deposits by bringing S-undersaturated mafic and ultramafic magmas to S-saturation (Lightfoot et al. 1990, 1993, 1994; Naldrett et al. 1992, 1995; Brugmann et al. 1993; Wooden et al. 1993; Hawkesworth et al. 1995; Lightfoot and Keays 2005). Crustal materials have high concentrations of large ion lithospheric elements. Relative to primitive magmas, contaminated magmas have low $\varepsilon_{Nd}(t)$ values and high Zr/Nb and Th/Nb ratios. Mantle-derived magmas from oceanic settings and mantle xenoliths are characterized by high $\varepsilon_{Nd}(t)$ values and low Zr/Nb and Th/Nb ratios. The large variation of Zr/Nb ratios and the low $\varepsilon_{Nd(260\ Ma)}$ values of the Yangliuping basalts cannot be

explained by fractional crystallization (Table 1; Fig. 4). Most samples of the Lower and Upper Units have Ta/La ratios of ~0.06 and define a trend (Trend 1) similar to that of the primitive mantle, which has an average Ta/La ratio of 0.06 (Wood et al. 1979), implying that the magmas that formed these rocks were dominantly controlled by fractionation (Fig. 13a). In contrast, most samples of the Middle Unit have much lower Ta/La ratios (0.03–0.04), indicating obvious crustal contamination (Trend 2, Fig. 13a). The Middle Unit shows consistently strongly negative Nb- and Ta-anomalies, also suggesting extensive crustal contamination (Fig. 6b).

Most lavas of the Middle Unit have low Nb/Y and high Zr/Nb ratios and plot along Trend 2 in Fig. 13b. Trend 2 extends to the average compositions of the lower crust (Weaver and Tarney 1984) and the nearby Kangding and Gezong basement complexes, indicating that the crystalline basement was probably an important contaminant (Zhou et al. 2002c). Some samples of the Lower Unit and Subunits 1 and 2 of the Upper Unit plot on the same trend with the Middle Unit (Fig. 13b); however, their high Ta/La ratios (~0.06) (Fig. 13a) suggest that their parental magmas were only weakly contaminated by the lower crust. Trend 1 extends toward the average of the upper crust with low Zr/Nb and high Nb/Y ratios, indicating only slight contamination of the upper crust (Fig. 13b).

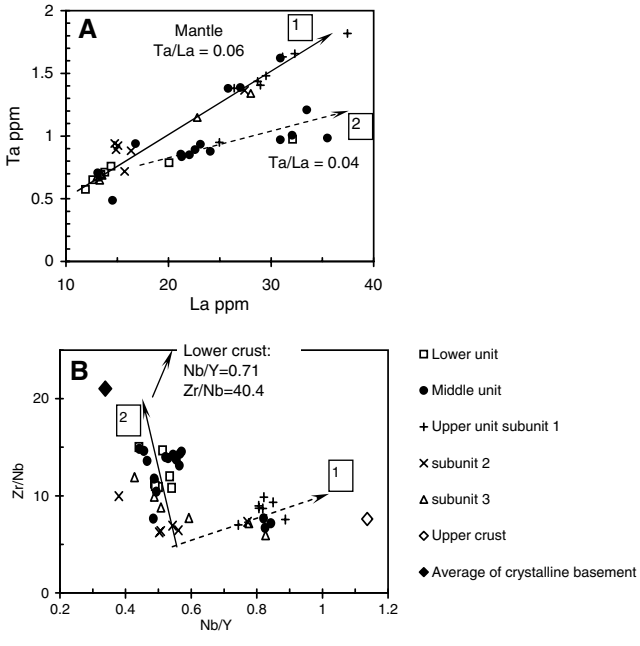

Fig. 13 Scattergrams demonstrating crustal contamination trends. **a** Ta vs La and **b** Zr/Nb vs Nb/Y. Trend 1 has Ta/La ratios similar to that of the mantle and shows weak contamination. Trend 2 is toward the lower crust and the average composition of the crystalline basement of the western Yangtze Block and present lower crustal contamination. The average compositions of the upper and lower crust are after Taylor and McLennan (1985) and Weaver and Tarney (1984), respectively

In summary, the main process that affected the precursor magmas of the Lower and Upper Unit basalts was fractional crystallization of the basaltic magmas accompanied by slight assimilation of crustal material. By contrast, the majority of the Middle Unit basalts are products of both extensive fractional crystallization and crustal assimilation.

PGE as indicators of S-saturation

Platinum and Pd are strongly chalcophile and incompatible elements during fractional crystallization of S-undersaturated magmas (Keays and Davidson 1976; Keays 1982, 1995; Barnes et al. 1985; Peck and Keays 1990), and have extremely high sulfide/silicate liquid partition coefficients in the order of 10^3–10^5, which are much higher than that those of Ni or Cu (Stone et al. 1990; Peach et al. 1990; Fleet et al. 1991; Bezmen et al. 1994). Thus, Pt and Pd can be efficiently extracted from magmas by minute amounts of segregating sulfide droplets. A high PGE concentration in lavas therefore is a good indicator for S-undersaturation, whereas very low PGE concentrations imply an early removal of sulfide melt. Model calculations indicate that the very significant chalcophile metal depletion of the Nadezhdinsky Formation in the Noril'sk area resulted from segregation as little as 0.1% sulfide (Lightfoot and Keays 2005).

In contrast, Ni and Cr are compatible elements that are removed from magmas by early crystallizing minerals (olivine and chromite, respectively) and hence decrease during fractional crystallization of S-undersaturated magmas. Whereas Pd is highly incompatible under these conditions (Keays 1995; Momme et al. 2002), Pt is moderately compatible as it is removed in spinels, especially chromite (Peck and Keays 1990). Thus, under S-undersaturated conditions, fractionation of magma should lead to a decrease in Ni/Pd ratios with increasing Pd/Cr, whereas Pt/Y ratios should either remain constant (if chromite is not a fractionating phase) or decrease slightly because Y is strongly incompatible. However, if segregation of immiscible sulfide-liquid occurs, Ni/Pd ratios increase in the residual magmas together with dramatic decreases of the Pd/Cr and Pt/Y ratios. Samples of the Yangliuping basalts whose parent magmas underwent silicate fractionation accompanied by minor sulfide fractionation exhibit a gentle decrease in Ni/Pd ratios as Pd/Cr ratios increase (Fig. 14a); however, those samples (mainly the Middle Unit basalts) whose parent magmas underwent more extensive sulfide fractionation exhibit a much more rapid decrease in Ni/Pd ratios with increasing Pd/Cr ratios. Although all of the Middle basalts lie along the sulfide fractionation path (SAFC), this may be fortuitous.

In contrast to Ni/Pd ratios, the Pt/Y ratios of the rocks whose parent magmas underwent mainly silicate fractionation accompanied by the removal of ~0.01% sulfides remain constant with decreasing Pd/Cr ratios

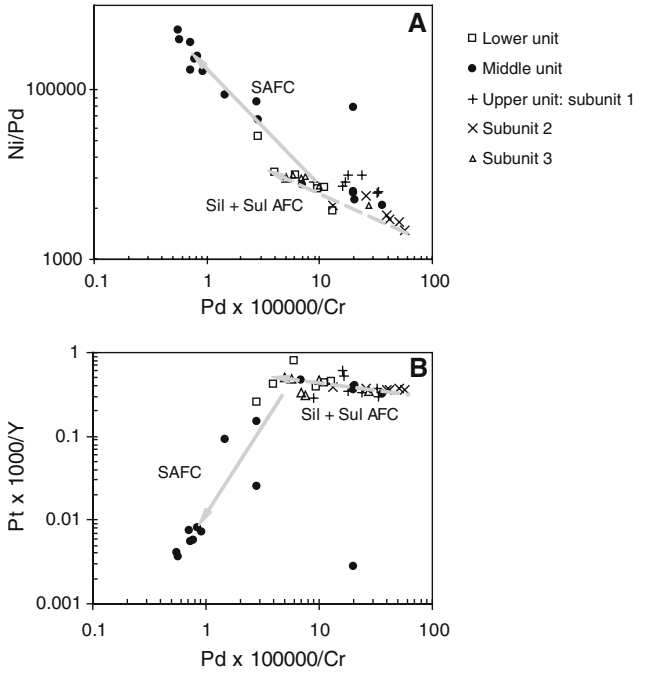

Fig. 14 Scattergrams of Ni/Pd vs Pd×100,000/Cr (**a**) and Pt×1,000/Y vs Pd×100,000/Cr (**b**) demonstrating variations due to AFC processes involving removal of small quantities of sulfides (*Sil + Sul AFC*) and larger quantities of sulfides (*SAFC*). See Fig. 12 caption for definition of *Sil + Sul AFC* and *SAFC*. The concentrations of Pt and Pd less than the detection limits are treated as 0.1 ppb in the plotting

(Fig. 14b). This suggests that unlike Pd, only minimal amounts of Pt were removed in the fractionating phases during the silicate fractionation processes which affected the Lower and Upper Unit basalts. The reason for this is that the Ernst Partition coefficient of Pd (=Pd in sulfide melt/Pd in silicate melt) is considerably higher than that of Pt (Vogel and Keays 1997). A dramatic decrease in Pt/Y ratio is observed in those Middle Unit basalts that underwent significant Pd loss (Fig. 14b). Both the significant increase in Ni/Pd ratios and the decrease in Pt/Y ratios with decreasing Pd/Cr ratios suggest significant removal of immiscible sulfide melt from the parent magmas of some of the Middle Unit basalts.

Key factors controlling S-saturation

Naldrett et al. (1992), Brugmann et al. (1993), and Lightfoot and Keays (2005) proposed that the low Ni, Cu, and PGE contents of the Nadezhdinsky Formation of the Siberian Traps, that is associated with the Noril'sk–Talnahk Ni–Cu–(PGE) sulfide deposits, are due to crustal contamination of primitive mafic magma. These authors suggested that the contamination event happened in a deep-seated staging magma chamber and that it led to the formation of low tenor magmatic sulfides; the magma in the staging chamber was replenished by primitive, chalcophile metal undepleted magma that reacted with the sulfides in the staging chamber and upgraded these to the high tenors of the Ni–Cu–(PGE) sulfides now found in the subvolcanic sills. Eventually, the staging chamber was emptied and the high tenor magmatic sulfides in it were emplaced into the subvolcanic sills. However, Arndt et al. (2003) have noted that other subvolcanic sills (e.g., the Lower Talnahk) underlying the Siberian Traps, which are believed to have formed from the same magmas have high γ Os_i (+40) values, whereas, the mineralized subvolcanic sills have low γ Os_i values ($\sim$+6). These authors thus concluded that the Ni, Cu, and PGE in the Noril'sk–Talnahk deposits could not have been derived from the magmas that formed the Nadezhdinsky Formation. Arndt et al. (2003) suggested that the deposits formed in their present locations as a result of the primitive magma assimilating S from the evaporite sediments which lie below the mineralized sills. This would account for the heavy S ($\delta^{34}S = +12$) observed by Grinenko (1985). However, Ripley et al. (2003) found that the Nadezhdinsky Formation basalts have mantle-like S isotope ratios; hence, the addition of the heavy S ($\delta^{34}S = +22$) from the evaporite could not have been the process that triggered the formation of the Ni–Cu–(PGE) sulfides. Mass balance considerations (cf. Burnham et al. 1999) would suggest that the ore sulfides should have low γ Os_i values. Although the crustal contaminant assimilated by the magma in the staging chamber proposed by Brugmann et al. (1993) and Lightfoot and Keays (2005) would probably have had very high γ Os_i values as noted by Arndt et al. (2003), the amount of (radiogenic) Os in the crustal material assimilated would have been trivial in comparison to the amount of (non-radiogenic) Os in the primitive magmas replenishing the staging chamber.

Sulfur solubility increases with increasing FeO and decreasing SiO_2 in mafic magmas (Haughton et al. 1974; Irvine 1975; Naldrett 1989). Therefore, fractionation may also be important for either inducing S-saturation in mafic magma or bringing it closer to a S-saturated state. It is difficult to estimate the solubility of S in a magma during the early stages of fractionation when olivine and chromite are the main crystallizing phases. Fractionation of these minerals can cause an increase in both FeO and SiO_2 in the residual melt. However, fractionation of pyroxene and Fe-bearing oxides would result in a decrease in FeO and an increase in SiO_2 in the residual melt and might cause S-saturation. Thermodynamic calculations indicate that about 20% crystallization of mafic minerals (olivine + orthopyroxene + spinel) could cause basaltic magma to become S-saturated (Li et al. 2001). The wide range of Pd/Pt ratios (0.45–2.0) of the Siberian Traps in the Noril'sk–Talnakh region is attributed to fractionation of sulfide-undersaturated primitive magmas (Lightfoot and Keays 2005). Although this did not induce S-saturation of the magmas, they were probably closer to a S-saturated state when they subsequently interacted with crustal rocks and became S-saturated in a staging chamber (Lightfoot and Keays 2005). Chalcophile and siderophile element concentrations of the Siberian basalts drop

suddenly below detection limits when MgO decreases to less than 8 wt% over a very constricted range (< 1 wt%) (Brugmann et al. 1993; Li et al. 2003; Lightfoot and Keays 2005).

In the Yangliuping area, the drop in PGE concentrations in the Middle Unit as Zr/Nb ratios increase and Cr and MgO contents decrease to less than 100 ppm and 8 wt%, respectively, indicates that both crustal contamination and fractional crystallization played a key role for S-saturation of the magmas in the staging chamber (Figs. 8, 15, 16). As in the case of the Siberian Traps basalts, the wide range of the Pd/Pt ratios of the Yangliuping basalts indicates that they underwent significant fractionation (Fig. 11); however, the fractionation history recorded by the Yangliuping basalts occurred mainly under mildly S-saturated conditions. The high Pd contents as well as the high Pd/Pt ratios of the least PGE-depleted and crustally contaminated Yangliuping basalts indicate that the magmas that formed the basalts must have undergone a significant period of fractionation; the least PGE-depleted Yangliuping basalt sample has a Pd/Pt ratio of 2.23 whereas the mantle has an average Pd/Pt ratio of 0.55 (Naldrett and Duke 1980). The prior fractionation history of the Yangliuping precursor magmas would have increased their S contents and rendered them easier to S-saturate when they became crustally contaminated.

Figures 4 and 10b show that the PGE concentrations of the Yangliuping basalts decrease with decreasing ε_{Nd} values. On the diagram of Nb/La vs ε_{Nd}, the Lower and Upper Units have the Nb/La ratios similar to that of the primitive mantle and ε_{Nd} values between that of the primitive mantle and MORB (Fig. 10a). This is consistent with the plots of Fig. 13a that the Lower and Upper Unit basaltic magmas underwent weak crustal contamination. The Middle Unit and the intrusive rocks, on the other hand, have ε_{Nd} values obviously lower than those of the Lower and Upper Units, indicating that both the Middle Unit and intrusive rocks were formed from extensively contaminated melts. Crystallization of oxides, e.g., magnetite and ilmenite, in the sills prior to eruption caused the Nb/La values of the intrusive rocks

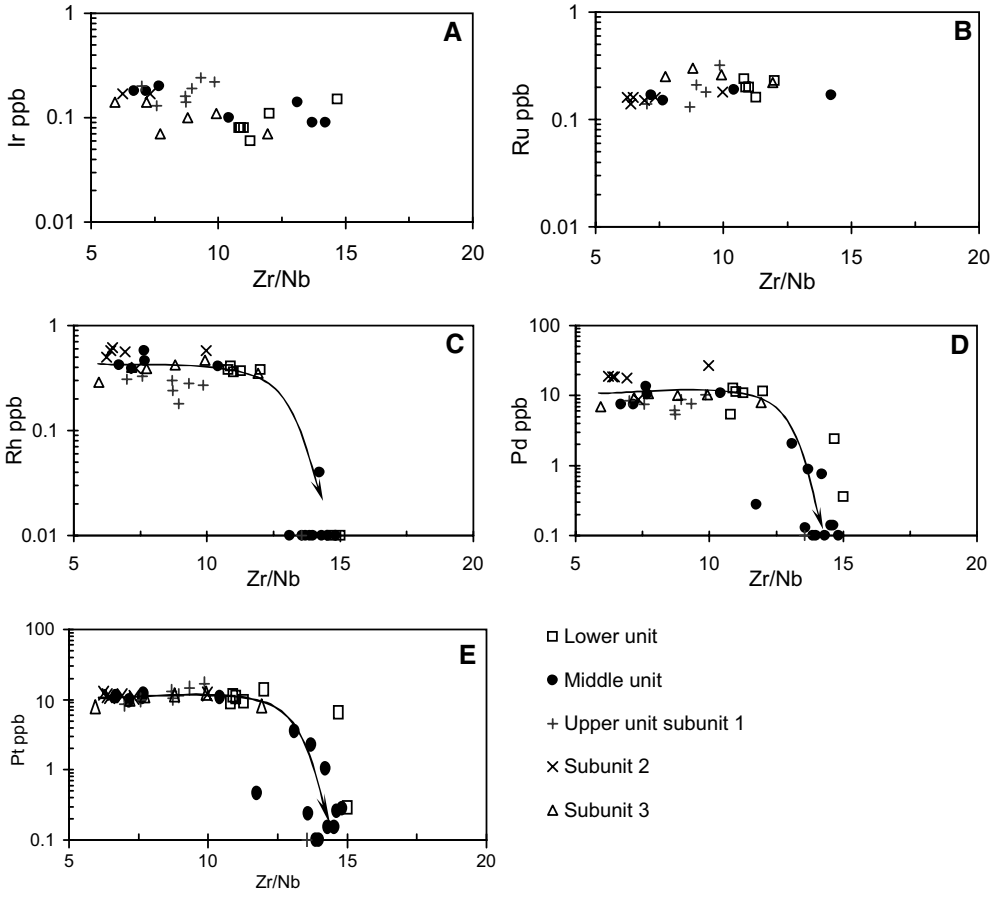

Fig. 15 Variation of PGE vs Zr/Nb. **a** Ir vs Zr/Nb, **b** Ru vs Zr/Nb, **c** Rh vs Zr/Nb, **d** Pd vs Zr/Nb, and **e** Pt vs Zr/Nb. Because Zr/Nb ratios should decrease with fractionation, the major cause of the increase in Zr/Nb ratios is increasing degrees of contamination. The dramatic decrease in PGE values once Zr/Nb ratios exceed c. 12.5 is probably due to assimilation of a more S-rich contaminant. The concentrations of Pt and Pd less than the detection limits are treated as 0.1 ppb, and that of Rh less than 0.08 ppb are plotted as 0.01 ppb, in these diagrams

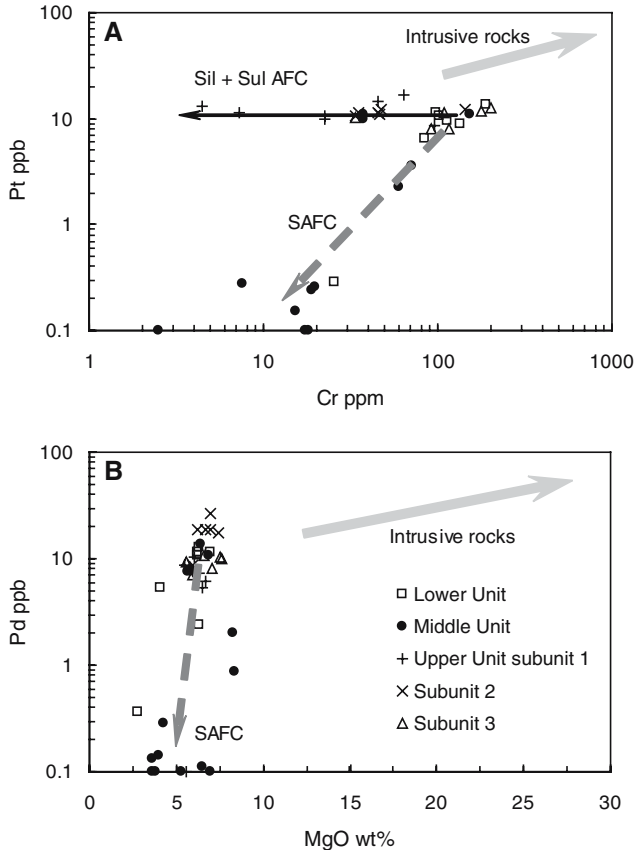

Fig. 16 **a** Correlation between Pt and Cr in the Yangliuping basalts showing the trends of basalts which experienced sulfide segregation and fractionation without sulfide segregation. **b** Palladium values drop sharply at MgO contents less than 8 wt%. The concentrations of Pt and Pd less than the detection limits are treated as 0.1 ppb in the plotting

to be higher than those of the Middle Unit (Fig. 10a). In addition, the correlation between low Pd concentrations in the Middle Unit basalts and their low $\varepsilon_{Nd(260\ Ma)}$ values strongly indicate a link between sulfide segregation and crustal contamination (Fig. 10b).

The nature of the crustal material which contaminated the magmas which the PGE-depleted Middle Unit basalts were probably different from that contaminated the remaining Middle Unit basalts as well as the Lower and Upper Unit basalts. Both Pt and Pd contents of the PGE-depleted Middle Unit basalts drop rapidly with increasing Zr contents and therefore increasing fractionation and contamination of the magma (Fig. 12). However, the Pt and Pd contents of the mildly PGE-depleted basalts do not decrease rapidly with Zr contents greater than 150 ppm Zr. This suggests that the nature of the contaminant in the two cases was different. We suggest that the crustal material which contaminated the PGE-depleted Middle Unit basalts contained a significant amount of S and it was the assimilation of this S-bearing crustal material that led to the segregation of larger amounts of magmatic sulfides from the magmas that produced the PGE-depleted Middle Unit basalts.

Integrated model

Based on this study, a coherent petrogenetic model relating the ECFB and the Ni–Cu–(PGE) sulfide ore deposits in the Yangliuping area is presented in Fig. 17.

Upwelling of the Emeishan mantle plume initiated extensive partial melting in the head of the plume beneath the western margin of the Yangtze Block and produced S-undersaturated and PGE-undepleted basaltic magmas as a result of partial melting at different depths in the plume. The majority of the partial melts were produced from garnet lherzolite at depths of >60–70 km but a few batches of magma resulted from partial melting of spinel lherzolite at depths <60 km.

The partial melts so produced entered a number of staging chambers at different levels in the crust: in some cases the staging chambers developed within the crystalline basement of the lower crust but in other cases they developed in upper crustal rocks. In both cases, the magmas underwent significant interaction with the crustal rocks as well as fractionation through AFC processes. These processes drove the magmas towards S-saturation which in some cases was only mild and as a consequence the magmas lost small (~0.01%) quantities of sulfides and minimal amounts of the PGE. In other cases, larger quantities of sulfides were lost and as a result, there was significant PGE loss. The magmas were subsequently erupted to form the lavas of the Lower, Middle and Upper Units, each of which contain lavas formed by magmas that underwent AFC processes in both types of staging chambers. The exception to this is the lavas of the Lower Unit, which were formed exclusively by magmas that had been processed in the lower crustal staging chambers.

In the case of most Middle Unit lavas and one of the Subunit 1 lavas, the magmas which had undergone AFC processes and had already become mildly S-saturated reacted with a crustal component that contained larger concentrations of S; the assimilation of this S-bearing component promoted the segregation of larger quantities of magmatic sulfides and therefore PGE depletion of the magmas.

Conclusions

The well-developed Permian flood basalt sequence in the Yangliuping region is part of the ELIP and includes three units showing temporal evolution of the basaltic magmatism with implication for sulfide segregation. The primary magmas were S-undersaturated and were derived by partial melting at variable depths in the upper mantle. The primary magmas entered staging chambers in the lower and upper crust where they underwent AFC processes which caused fractionation of the magmas and increased their S content to the point of mild S-saturation and as a result 0.01% magmatic sulfides coprecipitated along with the silicate and oxide fractionating phases. In some cases, having achieved mild S-saturation, some of

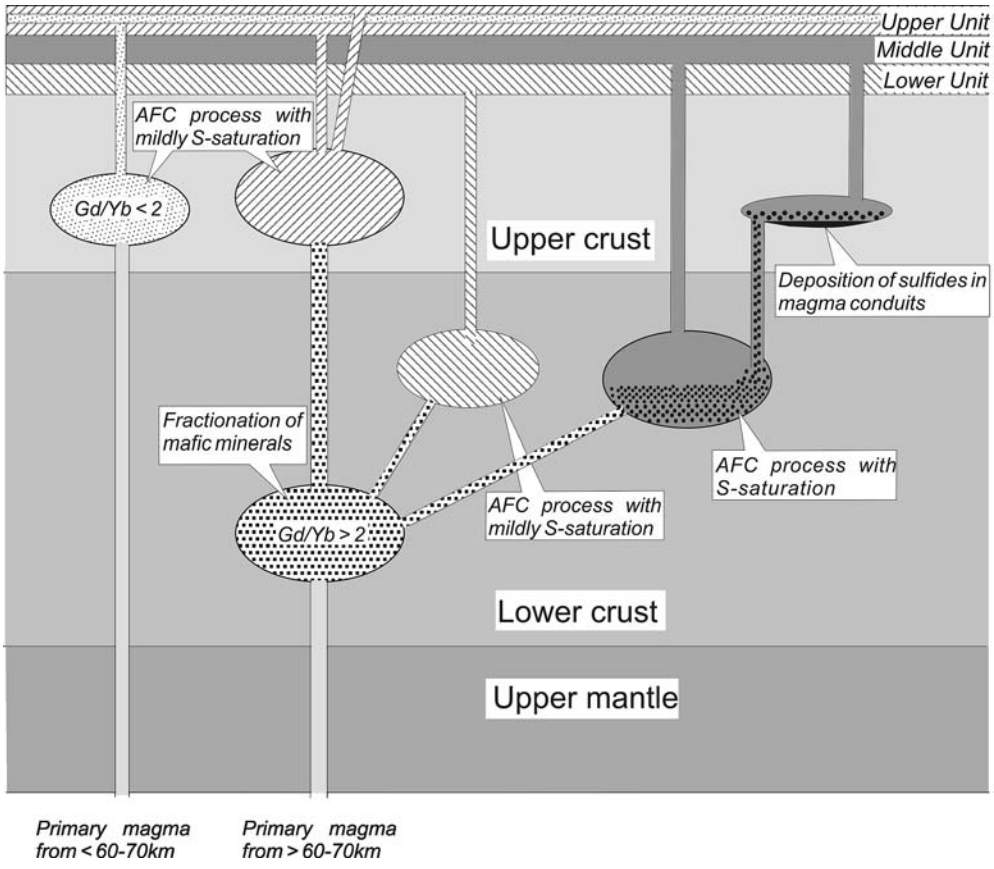

Fig. 17 A petrogenetic model showing the formation of the Permian basalt sequence at Yangliuping and the genetic link of the basalts with Ni–Cu–(PGE) sulfide mineralization in the mafic–ultramafic sills

batches of magma interacted with a crustal component that contained a significant amount of crustal S; as a result, these magmas became more heavily S-saturated, precipitated larger quantities of magmatic sulfides, and underwent significant PGE loss.

After processing in the deep-seated magma chambers, the different magmas were eventually erupted to form the basalts of the Lower, Middle, and Upper Units. In addition, the magmatic sulfides which had segregated from the magma batches that had undergone the greatest PGE losses (i.e., the majority of the Middle Unit basalts) where entrained in one of the magmas and emplaced into the subvolcanic Yangliuping and Zhengziyanwuo sills.

Acknowledgments This study was funded by the Research Grant Council of the Hong Kong SAR, China (HKU7056/03P and HKU7057/05P), research grants from China (NSFC 40373030 and "CAS Hundred Talents" Project from Chinese Academy of Sciences to X.-Y. Song). We gratefully acknowledge the kind help of Mr Luo Fu-Xun, Mr Zhu Ting-Guo, Mr Chen Jia-Zhong, and other members of the 402 Geological Team of Sichuan Province, China, during our field investigation. Xiao Fu is thanked for her help with the chemical analyses. The manuscript benefited from discussions with Christian Ihlenfeld. We thank P.T. Robinson and P. Momme for their constructive reviews.

References

Ali JR, Thompson GM, Song X-Y, Wang Y-L (2002) Emeishan Basalts (SW China) and the "end-Guadalupian" crisis; magneto-biostratigraphic constraints. J Geol Soc London 159:21–29

Arndt NT, Teixeira NA, White WM (1989) Bizarre geochemistry of Komatiites from the Crixas greenstone belt, Brazil. Contrib Mineral Petrol 101:187–197

Arndt NT, Czamanske GK, Walkerm RJ, Chauvel C, Fedorenko VA (2003) Geochemistry and origin of the intrusive hosts of the Noril'sk–Talnakh Cu–Ni–PGE sulfide deposits. Econ Geol 98:495–515

Arth JG (1976) Behaviors of trace elements during magmatic processes—a summary of theoretical models and their applications. J Res US Geol Surv 4:41–47

Barnes SJ, Naldrett AJ, Gorton MP (1985) The origin of the fractionation of platinum-group elements in terrestrial magmas. Chem Geol 53:303–323

Bezmen NS, Asif M, Brugmann GE, Romamekno IM, Naldrett AJ (1994) Experimental determinations of sulfide-silicate partitioning of PGE and Au. Geochim Cosmochim Acta 58:1251–1260

Brugmann GE, Naldrett AJ, Asif M, Lightfoot PC, Gorbachev NS, Fedorenko VA (1993) Siderophile and chalcophile metals as tracers of the evolution of the Siberian Trap in the Noril'sk region, Russia. Geochim Cosmochim Acta 57:2001–2018

Burnham OM, Lesher CM, Keays RR (1999) Geochemistry of mafic–ultramafic complexes and associated basalts in the Raglan block. In: Lesher CM (ed) Komatiitic Peridotite-hosted Fe–Ni–Cu–(PGE) Sulphide deposits in the Raglan area, Cape Smith Belt, New Québec. Guidebook series, vol. 2. Mineral Exploration Research Centre, Laurentian University, Sudbury, ON, pp. 159–173

Chung SL, Jahn BM (1995) Plume–lithosphere interaction in generation of the Emeishan flood basalts at the Permian–Triassic boundary. Geology 23:889–892

Fleet ME, Stone WE, Crocket JH (1991) Partitioning of palladium, iridium, and platinum between sulfide liquid and basaltic melt: effects of melt composition, concentration, and oxygen fugacity. Geochim Cosmochim Acta 55:2545–2554

Fujimaki H, Tatsumoto M, Aoki K (1984) Partition coefficients of Hf, Zr and REE between phenocrysts and groundmasses.

In: Proceeding of the 14th lunar and planetary science conference. J Geophys Res 89(Pt 2):B662–B672
Gibson SA, Thompson RN, Dickin AP, Leonardos OH (1996) Mafic potassic magmatic key to plume-lithosphere interactions and continental flood-basalts. Earth Planet Sci Lett 141:325–341
Green TH, Pearson NJ (1986) Rare earth element partitioning between sphene and coexisting silicate liquid at high pressure and temperature. Chem Geol 55:105–119
Grinenko LN (1985) Source of sulfur of the nickeliferous and barren gabbro–dolerite intrusions of the northwest Siberian platform. Int Geol Rev 27:695–708
Guo F, Fan WM, Wang YJ, Li CW (2004) When did the Emeishan mantle plume activity start? Geochronological and geochemical evidence from ultramafic–mafic dikes in southwestern China. Int Geol Rev 46:226–234
Haughton DR, Roeder PL, Skinner BJ (1974) Solubility of sulfur in mafic magma. Econ Geol 69:451–467
Hawkesworth CJ, Lightfoot PC, Fedorenko VA, Blake S, Naldrett AJ, Doherty W, Gorbachev NS (1995) Magma differentiation and mineralization in the Siberian continental flood basalts. Lithos 34:61–88
Hofmann AW (1988) Chemical differentiation of the earth: the relationship between mantle, continental crust, and oceanic crust. Earth Planet Sci Lett 90:297–314
Irvine TN (1975) Crystallization sequences of the Muskox intrusion and other layered intrusions-II Origin of chromitite layers and similar deposits of other magmatic ores. Geochim Cosmochim Acta 39:991–1020
Jackson SE, Fryer BJ, Gosse W, Healey DC, Longerich HP, Strong DF (1990) Determination of precious metals in geological materials by inductively coupled plasma-mass spectrometry (ICP-MS) with nickel sulfide fire-assay collection and tellurium coprecipitation. Chem Geol 83:119–132
Jenner GA, Longerich HP, Jackson SE, Fryer BJ (1990) ICP-MS—a powerful tool for high precision trace element analyses in earth sciences: evidence from analyses of selected USGS reference samples. Chem Geol 83:133–148
Keays RR (1982) Palladium and iridium in komatites and associated rocks: application to petrogenetic problems. In: Arndt NT, Nisbet EG (eds) Komatiiites. Allen and Unwin, Hemel Hempstead, pp 435–457
Keays RR (1995) The role of komatiitic and picritic magmatism and S-saturation in the formation of ore deposits. Lithos 34:1–18
Keays RR, Davidson RM (1976) Palladium, iridium and gold in the ores and host rocks of nickel sulfide deposits in Western Australia. Econ Geol 71:1214–1228
Lesher CM, Arndt NT (1995) REE and Nd isotop geochemistry, petrogenesis, and volcanic evolution of contaminated komatiites as Kambalda, Western Australia. Lithos 34:127–157
Lesher CM, Burnham OM, Keays RR (2001) Trace-element geochemistry and petrogenesis of barren and ore-association komatiites. Can Mineral 39:673–696
Li C, Maier WD, Waal SAD (2001) The role of magma mixing in the genesis of PGE mineralisation in the Bushveld complex: thermodynamic calculation and new interpretations. Econ Geol 96:653–662
Li C, Ripley EM, Naldrett AJ (2003) Compositional variations of olivine and sulfur isotopes in the Noril'sk and Talnakh intrusions, Siberia: implications for ore-forming processes in dynamic magma conduits. Econ Geol 98:69–86
Lightfoot PC, Hawkesworth CJ (1997) Flood basalts and magmatic Ni, Cu and PGE sulphide mineralization: comparative geochemistry of the Noril'sk (Siberian Traps) and West Greenland sequence. In: Mahoney JJ, Coffin MF (eds) Large Igneous Provinces: oceanic, and planetary flood volcanism, Geophysical Monograph 100. American Geophysical Union, pp 357–380
Lightfoot PC, Keays RR (2005) Siderophile and chalcophile metal variations in flood basalts from the Siberian Trap, Noril'sk region: implication for the origin of the Ni–Cu–PGE sulfide ores. Econ Geol 100:439–462
Lightfoot PC, Naldrett AJ, Gorbachev NS, Doherty W, Fedorenko VA (1990) Geochemistry of the Siberian Trap of the Noril'sk Aream USSR, with implications for the relative contributions of crustal and mantle to flood basalt magmatism. Contrib Mineral Petrol 104:631–644
Lightfoot PC, Hawkesworth CJ, Hergt J, Naldrett AJ, Gorbachev NS, Fedorenko VA (1993) Remobilisation of the continental lithosphere by a mantle plume: major-, trace-element and Sr-, Nd-, and Pb-isotope evidence from picritic and tholeiitic lavas of the Noril'sk District, Siberian Trap, Russia. Contrib Mineral Petrol 114:171–188
Lightfoot PC, Hawkesworth CJ, Hergt J, Naldrett AJ, Gorbachev NS, Fedorenko VA, Doherty W (1994) Chemostratigraphy of Siberian trap lavas, Noril'sk District, Russia: implication for the evolution of flood basalt magmas. In: Lightfoot PC, Naldrett AJ (eds) The Sudbury–Noril'sk symposium. The Sudbury–Noril'sk symposium, special volume Ontario geological survey, vol. 5, pp 283–312
Momme P, Tegner C, Brooks CK, Keays RR (2002) The behaviour of platinum-group elements in basalts from the East Greenland rifted margin. Contrib Mineral Petrol 143:133–153
Momme P, Tegner C, Brooks CK, Keays RR (2005) Two melting regimes during Paleogene flood basalt generation in East Greenland: combined REE and PGE modeling. Contrib Mineral Petrol 151:88–100
Naldrett AJ (1989) Magmatic sulfide deposits. Clarendon, New York, p 186
Naldrett AJ, Duke JM (1980) Platinum metals in magmatic sulfide ores. Science 208:1417–1428
Naldrett AJ, Lightfoot PC, Fedorenko VA, Doherty W, Gorbachev NS (1992) Geology and geochemistry of intrusions and flood basalts of the Noril'sk region, USSR, with implication for the origin of the Ni–Cu ores. Econ Geol 87:975–1004
Naldrett AJ, Fedorenko VA, Lightfoot PC, Kunilov VI, Gorbachev NS, Doherty W, Johan Z (1995) Ni–Cu–PGE deposits of the Noril'sk region, Siberia: their formation in conduits for flood basalt volcanism. Trans Inst Mining Metallurgy 104:B1–B86
Nielson RL, Gallahan WE, Newberger F (1992) Experimental determined mineral-melt partition coefficients for Sc, Y and REE for olivine, orthopyroxene, pigeonite, magnetite and ilmenite. Contrib Mineral Petrol 110:488–499
Pauling L (1960) Nature of the chemical bond, 3rd edn. Cornell University Press, Ithaca
Peach CL, Mathez EA, Keays RR (1990) Sulfide melt–silicate melt distribution coefficients for noble metals and other chalcophile elements reduced from MORB: implications for partial melting. Geochim Cosmochim Acta 54:3379–3389
Peck DC, Keays RR (1990) Insights into the behaviour of precious metals in primitive, S-undersaturated magmas: evidence from the Heazlewood river complex, Tasmania. Can Mineral 28:553–577
Ripley EM, Lightfoot PC, Li C, Elswick ER (2003) Sulfur isotopic studies of continental flood basalts in the Noril'sk region: implications for the association between lavas and ore-bearing intrusions. Geochim Cosmochim Acta 67:2805–2817
Rollinson HR (1993) Using geochemical data: evolution, presentation, interpretation. Longman Group UK Limited, Singapore
Song X-Y, Zhou M-F, Hou Z-Q, Cao Z-M, Wang Y-L, Li Y-G (2001) Geochemical constraints on the mantle source of the Upper Permian Emeishan continental flood basalts, Southwestern China. Int Geol Rev 43:213–225
Song X-Y, Zhou M-F, Cao Z-M, Sun M, Wang Y-L (2003) Ni–Cu–(PGE) magmatic sulfide deposits in the Yangliuping area, Permian Emeishan igneous province, SW China. Miner Deposita 38:831–843
Song X-Y, Zhou M-F, Cao Z-M, Robinson PT (2004a) Late Permian rifting of the South China Craton caused by the Emeishan mantle plume?. J Geol Soc London 161:773–781
Song X-Y, Zhou M-F, Cao Z-M (2004b) Genetic relationships between base metal sulfides and platinum-group minerals in the Yangliuping Ni–Cu–(PGE) sulfide deposit, Southwestern China. Can Mineral 42:469–483

Song X-Y, Zhang C-J, Hu R-Z, Zhong H, Zhou M-F, Ma R-Z, Li Y-G (2005a) Genetic links of magmatic deposits in the Emeishan large igneous province with dynamics mantle plume (in Chinese with English abstract). J Mineral Petrol 25(4): 35–44

Song X-Y, Zhong H, Zhou M-F, Tao Y (2005b) Magmatic sulfide deposits in the Permian Emeishan Large Igneous Province, SW China. In: Mao JW, Bierlein FP (eds) Mineral deposit research: meeting the global challenge (the 8th Biennial SGA meeting in Beijing), vol. 1, pp 465–468

Stone WE, Crocket JH, Fleet ME (1990) Partitioning of palladium, iridium, platinum, and gold between sulfide liquid and basaltic melt at 1200°C. Geochim Cosmochim Acta 54:2341–2344

Taylor SR, McLennan SM (1985) The continental crust: its composition and evolution. Blackwell, London

Vogel DC, Keays RR (1997) The application of platinum group geochemisty in constraining the source of Basalt magmas: results from the newer volcanic province, Victoria, Australia. Chem Geol 136:181–204

Weast RC, Astle MJ, Beyer WH (1986) CRC handbook of chemistry and physics. CRC, Boca Raton

Weaver B, Tarney J (1984) Empirical approach to estimating the composition of the continental crust. Nature 310:575–577

Wood DA, Tarneu J, Varet J, Saunders AN, Bouhault H, Joron JL, Treuil M, Cann JR (1979) Geochemistry of basalts drills in the North Atlantic by IPOD Leg 49: implications for mantle heterogeneity. Earth Planet Sci Lett 42:77–97

Wooden JL, Czamanske GK, Fedorenko VA, Arndt NT, Chauvel C, Bouse RM, King BSW, Knight RJ, Siems DF (1993) Isotopic and trace-element constrains on mantle and crustal contributions to Siberian continental flood basalts, Noril'sk area, Siberia. Geochim Cosmochim Acta 57:3677–3704

Xu Y-G, Chung SL, Jahn BM, Wu G-Y (2001) Petrologic and geochemical constraints on the petrogenesis of Permian–Triassic Emeishan flood basalts in southwestern China. Lithos 58(3–4):145–168

Zhong H, Zhou X-H, Zhou M-F, Sun M, Liu, B-G (2002) Platinum-group element geochemistry of the Hongge Fe–V–Ti deposit in the Pan-Xi area, southwestern China. Miner Deposita 37: 226–239

Zhou M-F, Malpas J, Song X-Y, Robinson PT, Sun M, Kennedy AK, Lesher CM, Keays RR (2002a) A temporal link between the Emeishan Large Igneous Province (SW China) and the end-Guadalupian mass extinction. Earth Planet Sci Lett 196:113–122

Zhou M-F, Yang Z-X, Song X-Y, Keays RR, Lesher CM (2002b) Magmatic Ni–Cu–(PGE) sulfide deposits in China. In: Cabri LJ (ed) The geology, geochemistry, mineralogy, mineral beneficiation of the Platinum-Group Elements, vol. 54. Canadian Institute of Mining, Metallurgy and Petroleum, Canada, pp 619–636

Zhou M-F, Yan D-P, Kennedy AK, Li Y-Q, Ding J (2002c) SHRIMP U-Pb zircon geochronological and geochemical evidence for Neoproterozoic, arc magmatism along the western margin of the Yangtze Block, Yangtze. Earth Planet Sci Lett 196:51–67

Zhou M-F, Robinson PT, Lesher CM, Keays RR, Zhang CJ, Malpas J (2005) Geochemistry, petrogenesis and metallogenesis of the Panzhihua gabbroic layered intrusion and associated Fe–Ti–V oxide deposits, Sichuan Province, SW China. J Petrol 46:2253–2280

Zhou M-F, Zhao JH, Qi L, Su W, Hu RZ (2006) Zircon U–Pb geochronology and elemental and Sr–Nd isotopic geochemistry of Permian mafic rocks in the Funing area, SW China. Contrib Mineral Petrol 151:1–19